Verification Report OL V 7.0

SCIAMACHY Level 1b to 2 processing

ENV-VRP-QWG-SCIA-0095

Issue 4A

28 March 2018

Distribution List

Name	Affiliation	Copies	Name	Affiliation	Copies
SQWG					

Number of copies:

Author and Compilation List

	Name	Affiliation	Date	Signature
Author				
Compilation	S. Gretschany G. Lichtenberg	DLR-IMF	09/05/17 28/03/18	Günter Lichtenberg Digital signiert von Günter Lichtenberg DN: CN=Günter Lichtenberg, O=DLR, OU=IMF-ATP, E=guenter.lichtenberg@dlr.de, C=DE Grund: Ich bin der Verfasser dieses Dokuments Ort: Datum: 14-08-2018 14:32:49 Foxit Reader Version: 9.1.0

Change Record

Issue	Date	Page	Description of Change
1	20/08/08	all	completely new
2	05/11/09	all	Adjustments for Processor Version 5
3	07/07/14	all	Adjustments for Processor Version 6
3A	29/01/15	Several p. 57	• Adjustments for tropospheric column NO_2 • added section for tropospheric NO_2
4	20/09/16	All	Adjustments for Processor Version 7
4A	28/03/18	p. 5	Corrected previous processor version
		p. 6	Corrected reference to L2 ATBD
		p.10	Added remark about netCDF format
		p. 19	Adjusted figure for CIR
		p. 29	Moved Regression Test section to a position before the L2 step2 verification section
		p.31-34	Added additional figures and explanations for the investigation of a possible O3 trend
		p.41-42	Added a more detailed explanation of the AAI differences betweeb the usage og L1 V8 and V9, added a scatter plot for the residuals
		p. 43	Added better explanation for the cloud fraction differences in the step2 verification
		p.45-50	Added investigation of the L1 change impact on CO and justification for the L1 setting change
		p. 55-57	Added section on tangent height dependence of correlation and slope coefficients
		p. 57-61	Added results of the step 2 verification of Limb cloud algorithm
		p. 62	Updated Summary and conclusions

Table of Contents

1 Introduction

1.1 Purpose and Scope of the document

SCIAMACHY is a joint project of Germany, The Netherlands and Belgium for atmospheric measurements. SCIAMACHY had been selected by the European Space Agency (ESA) for inclusion in the list of instruments for Earth observation research for the ENVISAT polar platform, which has been launched in 2002. The SCIAMACHY programme is currently in Phase F under the supervision of the SCIAMACHY science team (SSAG), headed by the Principal Investigators Professor J. P. Burrows (University of Bremen, Germany), Professor I.A.A. Aben (SRON, The Netherlands) and Dr. C. Muller (BIRA, Belgium).

The Quality Working Group has been installed in 2007 to intensify the development and implementation of the Algorithm Baseline for the operational data processing system of SCIAMACHY. Current members of the QWG are the University of Bremen (IFE) (Lead), BIRA, DLR, and SRON. The expertise of KNMI is brought in via an association with SRON.

The purpose of this document is to report the results of the verification campaign carried out for the new version of the Level 2 processor for the Algorithm Baseline Update of the Level 1b-2 off-line data processing. The document is thought as a report to the European and national space agencies, namely European Space Agency (ESA), German Space Agency (DLR), and the Dutch counterpart (NSO), about the verification to provide a decision baseline for the implementation and integration of the new Algorithm Baseline in the operational ENVISAT ground segment.

The subject of this document is the verification of the Algorithm Baseline Update from version 6.01 to version 7 of the SCIAMACHY Level 1b-2 Off-line (SGP) data processing unit. In the new version of the processor, the following upgrades were introduced:

1. Tropospheric BrO column
2. Update of Limb-Cloud algorithm

1.2 Documents

1.2.1 Applicable Documents

Following documents are applicable for this technical note:

[A1] ENVISAT-1 Ground Segment Concept, ESA/PB-EO(94)75, Issue 5, 20 September 1994

[A2] ESA Software Engineering Standards, ESA PSS-05-0, Issue 2, Feb. 1991

[A3] ENVISAT Product Specification Volume 15, Rev. 3M

[A4] SCIAMACHY Processor Verification Plan, ENV-VPL-DLR-SCIA-0128, issue 1, 12.07.2016

1.2.2 References

[R1] Test Procedure Document/Test Data Set Definition SGP OL Level 2, ENV-TPD-DLR-SCIA-0072, Issue 4A, 21 October 2009

[R2] Algorithm Theoretical Baseline Document (SGP OL Version 7), ENV-ATB-QWG-SCIA-0085, issue 3, 2018

[R3] Eichmann K.-U., Lelli L., von Savigny C., Sembhi H., Burrows J.P. (2016). Global cloud top height retrieval using SCIAMACHY limb spectra: model studies and first results. *Atmos. Meas. Tech.* 9, 793-815

[R4] N. Theys, N., Van Roozendael, M., Hendrick, F., Yang, X., De Smedt, I., Richter, A., Begoin, M., Errera, Q., Johnston, P.V., Kreher, K., De Mazi`ere, M. (2011). Global observations of tropospheric BrO columns using GOME-2 satellite data. *Atmos. Chem. Phys.* 11, 1791-1811

1.3 Abbreviations and Acronyms

A list of abbreviations and acronyms which are used throughout this document is given below:

AAI	Absorbing Aerosol Index
ADF	Auxiliary Data File
ADS	Annotation Data Set
AMC	Air Mass Correction
AMF	Air Mass Factor
AMJ	April-May-June
AO	Announcement of Opportunity
ARD	Absolute Relative Difference
BIRA-IASB	Belgisch Instituut voor Ruimte-Aëronmie, Institut d'Aéronomie Spatiale de Belgique
CFI	Customer Furnished Items
CIR	Colour index ratio
CR	Change Request
DARA	Deutsche Agentur für Raumfahrtangelegenheiten
DB	Database
DFD	Deutsches Fernerkundungsdatenzentrum (DLR)
DLR	Deutsche Zentrum für Luft- und Raumfahrt e.V.
DS	Data set
ECMWF	European Centre for Medium Weather Forecast
ENVISAT	Environmental Satellite
EnviView	Viewing software package for ENVISAT data products
ESA	European Space Agency
GADS	Global Annotation Data Set
GOME	Global Ozone Monitoring Experiment
IMF	Institut für Methodik der Fernerkundung (DLR)
IPF	Instrument Processing Facility
IUP-UB	Institut für Umweltphysik der Universität Bremen
JAS	July-August-September
JFM	January-February-March
KNMI	Royal Netherlands Meteorological Institute
MDS	Measurement Data Set

MPH	Main Product Header
mrd	Mean relative difference
NCR	Non-Conformance Report
ND	Number Density
NSO	Netherlands Space Office
NLC	Noctilucent clouds
OND	October-November-December
PDS	Payload Data Segment
PPS	Profile Per State
PSC	Polar Stratospheric Clouds
RTM	Radiative Transfer Model
SCIAMACHY	Scanning Imaging Absorption Spectrometer for Atmospheric Chartography
SCD	Slant Column Density
SCODA	Cloud Detection Algorithm
SCR	Software Change Request
SGP	SCIAMACHY Ground Processor
SPICI	SCIAMACHY Polarisation Measurement Devices Identification of Clouds and Ice/Snow Method
SPF	Slant path factor
SPR	Software Problem Report
SQWG	SCIAMACHY Quality Working Group
SRON	Netherlands Institute for Space Research
SSAG	SCIAMACHY Science Advisory Group
SZA	Solar Zenith Angle
VCD	Vertical Column Density
WFMD(OAS)	Weighting Function Modified Differential (Optical Absorption Spectroscopy)

1.4 Document Overview

Details of the verification method are laid out in the verification plan [A4]. Then a short summary of processor changes follows in section 2. The following section describes the details of the verification for each processor change. There are two steps in the verification. The chapters for the first step of the verification are structured in the following way:

- **Introduction:** A more detailed description of the processor change
- **Involved Partners:** Point of contacts in case of questions
- **Verification Set-Up:** Description of the verification Method
- **Verification Data Set:** Description of the data sets used
- **Verification Results:** Results of the verification.

For the step 2 verification we group all the products in categories and then show the results for each product separately in a subsection for the operational and the reference algorithm (note that the latter might not be needed). The structure is as follows

- **X. Top Product Group:** E.g. "Nadir UV/VIS Trace gases"
- **X.Y Product:** E.g. "Ozone"
- **X.Y.1 Operational:** Showing comparisons for the operational algorithm
- **X.Y.2 Reference Algorithm** Showing results for the reference, if needed

At the end of the document a short summary and conclusions are given.

2 Summary of Changes

The version of the SCIAMACHY Level 1b-2 ground processor (SGP) under testing is Version 7. Compared to the V6 it includes tropospheric *BrO* columns as a new product; the limb cloud detection algorithm SCODA has been also updated following an update of the corresponding scientific product.

Besides that a public release of the new L2 Version7 dataset is planned to be done in a new user-friendly and more appropriate for the long-term data preservation NetCDF format. However , all verification procedures here presented are to be conducted using the original ENVISAT N1 format.. The netCDF product is then tested against the veridied ENVISAT product.

3 Verification plan

The verification purpose is to demonstrate that the scientific algorithms are correctly implemented into the operational processing chain. To do so the results obtained by the scientific algorithms are compared with those produced by the operational processor. Due to some constraints for the operational processing or peculiarities of the operational processor's architecture it is not always possible to ensure one-to-one implementation of a scientific algorithm. This inevitably leads to differences between operational and scientific results. Such deviations have to be explained and it has to be decided whether they are acceptable.

The verification procedure is performed using the verification data set: a number of orbits that has to be processed by the scientific and the operational processors and the results are compared. The verification orbits have been chosen according to the following criteria:

- good seasonal coverage (all seasons have to be represented equally);
- good coverage through the whole duration of mission: 2002 – 2012.

Growing from verification to verification the data set now consists of 216 orbits.

Table 3.1: *The verification data set:orbit numbers and corresponding L1v8 products. The new L1v9 are also used for testing.*

Orbit #	Level 1b Product
02209	SCI_NL__1PYDPA20020802_093420_000057082008_00151_02209_0000.N1
02321	SCI_NL__1PYDPA20020810_051658_000059332008_00263_02321_0000.N1
02946	SCI_NL__1PYDPA20020922_211146_000059542009_00387_02946_0000.N1
03358	SCI_NL__1PYDPA20021021_155758_000059312010_00298_03358_0000.N1
03502	SCI_NL__1PYDPA20021031_172353_000060152010_00442_03502_0000.N1
04520	SCI_NL__1PYDPA20030110_201324_000060152012_00458_04520_0000.N1
04618	SCI_NL__1PYDPA20030117_163251_000059612013_00055_04618_0000.N1
04673	SCI_NL__1PYDPA20030121_124504_000059822013_00110_04673_0000.N1
04720	SCI_NL__1PYDPA20030124_193330_000059612013_00157_04720_0000.N1
04757	SCI_NL__1PYDPA20030127_093541_000059382013_00194_04757_0000.N1
04812	SCI_NL__1PYDPA20030131_054818_000059382013_00249_04812_0000.N1
04830	SCI_NL__1PYDPA20030201_115858_000060212013_00267_04830_0000.N1
04953	SCI_NL__1PYDPA20030210_021227_000059772013_00390_04953_0000.N1
04995	SCI_NL__1PYDPA20030213_003742_000060092013_00432_04995_0000.N1
05033	SCI_NL__1PYDPA20030215_162052_000059662013_00470_05033_0000.N1
05147	SCI_NL__1PYDPA20030223_152900_000059832014_00083_05147_0000.N1
05202	SCI_NL__1PYDPA20030227_114155_000060062014_00138_05202_0000.N1
05257	SCI_NL__1PYDPA20030303_075437_000060172014_00193_05257_0000.N1
05326	SCI_NL__1PYDPA20030308_033623_000059702014_00262_05326_0000.N1
05373	SCI_NL__1PYDPA20030311_102423_000059332014_00309_05373_0000.N1

Orbit #	Level 1b Product
05411	SCI_NL__1PYDPA20030314_020647_000060172014_00347_05411_0000.N1
05482	SCI_NL__1PYDPA20030319_010920_000059732014_00418_05482_0000.N1
05636	SCI_NL__1PYDPA20030329_192131_000059682015_00071_05636_0000.N1
05677	SCI_NL__1PYDPA20030401_160721_000059352015_00112_05677_0000.N1
05789	SCI_NL__1PYDPA20030409_115325_000059792015_00224_05789_0000.N1
05845	SCI_NL__1PYDPA20030413_094713_000059792015_00280_05845_0000.N1
05859	SCI_NL__1PYDPA20030414_091529_000059792015_00294_05859_0000.N1
05972	SCI_NL__1PYDPA20030422_064249_000059902015_00407_05972_0000.N1
06027	SCI_NL__1PYDPA20030426_025607_000059862015_00462_06027_0000.N1
06197	SCI_NL__1PYDPA20030508_000258_000056592016_00131_06197_0000.N1
06298	SCI_NL__1PYDPA20030515_012255_000056852016_00232_06298_0000.N1
06467	SCI_NL__1PYDPA20030526_204328_000056472016_00401_06467_0000.N1
06468	SCI_NL__1PYDPA20030526_222404_000056792016_00402_06468_0000.N1
06505	SCI_NL__1PYDPA20030529_122606_000056472016_00439_06505_0000.N1
06534	SCI_NL__1PYDPA20030531_130323_000056782016_00468_06534_0000.N1
06586	SCI_NL__1PYDPA20030604_041422_000056782017_00019_06586_0000.N1
06649	SCI_NL__1PYDPA20030608_135157_000056462017_00082_06649_0000.N1
06651	SCI_NL__1PYDPA20030608_171309_000056462017_00084_06651_0000.N1
06739	SCI_NL__1PYDPA20030614_204544_000056462017_00172_06739_0000.N1
06810	SCI_NL__1PYDPA20030619_194811_000056802017_00243_06810_0000.N1
06881	SCI_NL__1PYDPA20030624_185041_000056502017_00314_06881_0000.N1
06935	SCI_NL__1PYDPA20030628_132301_000056522017_00368_06935_0000.N1
06991	SCI_NL__1PYDPA20030702_111635_000056542017_00424_06991_0000.N1
07076	SCI_NL__1PYDPA20030708_094735_000056902018_00008_07076_0000.N1
07103	SCI_NL__1PYDPA20030710_070348_000056592018_00035_07103_0000.N1
07201	SCI_NL__1PYDPA20030717_032244_000056972018_00133_07201_0000.N1
07286	SCI_NL__1PYDPA20030723_015356_000056692018_00218_07286_0000.N1
07399	SCI_NL__1PYDPA20030730_232204_000057082018_00331_07399_0000.N1
07480	SCI_NL__1PYDPA20030805_151059_000056802018_00412_07480_0000.N1
07505	SCI_NL__1PYDPA20030807_090605_000057132018_00437_07505_0000.N1
07831	SCI_NL__1PYDPA20030830_033631_000059802019_00262_07831_0000.N1
07834	SCI_NL__1PYDPA20030830_083809_000060042019_00265_07834_0000.N1
07884	SCI_NL__1PYDPA20030902_202746_000059642019_00315_07884_0000.N1
07896	SCI_NL__1PYDPA20030903_163503_000059652019_00327_07896_0000.N1
07993	SCI_NL__1PYDPA20030910_111410_000059362019_00424_07993_0000.N1
08077	SCI_NL__1PYDPA20030916_080347_000059752020_00007_08077_0000.N1
08161	SCI_NL__1PYDPA20030922_045448_000059312020_00091_08161_0000.N1
08231	SCI_NL__1PYDPA20030927_021533_000059742020_00161_08231_0000.N1

Orbit #	Level 1b Product
08330	SCI_NL__1PYDPA20031004_001602_000058872020_00260_08330_0000.N1
08401	SCI_NL__1PYDPA20031008_231804_000059342020_00331_08401_0000.N1
08422	SCI_NL__1PYDPA20031010_103030_000059712020_00352_08422_0000.N1
08449	SCI_NL__1PYDPA20031012_074712_000059342020_00379_08449_0000.N1
08483	SCI_NL__1PYDPA20031014_164626_000060182020_00413_08483_0000.N1
08582	SCI_NL__1PYDPA20031021_144611_000059742021_00011_08582_0000.N1
08666	SCI_NL__1PYDPA20031027_120208_000060362021_00095_08666_0000.N1
08707	SCI_NL__1PYDPA20031030_082053_000059742021_00136_08707_0000.N1
08835	SCI_NL__1PYDPA20031108_065742_000059342021_00264_08835_0000.N1
08877	SCI_NL__1PYDPA20031111_052250_000059662021_00306_08877_0000.N1
08903	SCI_NL__1PYDPA20031113_005833_000059662021_00332_08903_0000.N1
08913	SCI_NL__1PYDPA20031113_174436_000059662021_00342_08913_0000.N1
09057	SCI_NL__1PYDPA20031123_191039_000059832021_00486_09057_0000.N1
09127	SCI_NL__1PYDPA20031128_163232_000059612022_00055_09127_0000.N1
09168	SCI_NL__1PYDPA20031201_131645_000059832022_00096_09168_0000.N1
09189	SCI_NL__1PYDPA20031203_002955_000059612022_00117_09189_0000.N1
09253	SCI_NL__1PYDPA20031207_114757_000059822022_00181_09253_0000.N1
09309	SCI_NL__1PYDPA20031211_094209_000059612022_00237_09309_0000.N1
09336	SCI_NL__1PYDPA20031213_065709_000060262022_00264_09336_0000.N1
09391	SCI_NL__1PYDPA20031217_031011_000060272022_00319_09391_0000.N1
09816	SCI_NL__1PYDPA20040115_194539_000059612023_00243_09816_0000.N1
09987	SCI_NL__1PYDPA20040127_182730_000060002023_00414_09987_0000.N1
10584	SCI_NL__1PYDPA20040309_112444_000059692025_00009_10584_0000.N1
10597	SCI_NL__1PYDPA20040310_091242_000059332025_00022_10597_0000.N1
11382	SCI_NL__1PYDPA20040504_052223_000060032026_00306_11382_0000.N1
12521	SCI_NL__1PYDPA20040722_190912_000056432028_00443_12521_0000.N1
13328	SCI_NL__1PYDPA20040917_040756_000059922030_00248_13328_0000.N1
13560	SCI_NL__1PYDPA20041003_090641_000059522030_00480_13560_0000.N1
14226	SCI_NL__1PYDPA20041118_214525_000060282032_00144_14226_0000.N1
15049	SCI_NL__1PYDPA20050115_093838_000059912033_00466_15049_0000.N1
15783	SCI_NL__1PYDPA20050307_161743_000059952035_00198_15783_0000.N1
16884	SCI_NL__1PYDPA20050523_141702_000059962037_00297_16884_0000.N1
17574	SCI_NL__1PYDPA20050710_191429_000057092038_00486_17574_0000.N1
18499	SCI_NL__1PYDPA20050913_100425_000060032040_00409_18499_0000.N1
19811	SCI_NL__1PYDPA20051214_014935_000059922043_00218_19811_0000.N1
20693	SCI_NL__1PYDPA20060213_163755_000059392045_00098_20693_0000.N1
21754	SCI_NL__1PYDPA20060428_193304_000060232047_00157_21754_0000.N1
22306	SCI_NL__1PYDPA20060606_090800_000056942048_00208_22306_0000.N1

Orbit #	Level 1b Product
22330	SCI_NL__1PYDPA20060608_012219_000056942048_00232_22330_0000.N1
22331	SCI_NL__1PYDPA20060608_030255_000057342048_00233_22331_0000.N1
22332	SCI_NL__1PYDPA20060608_044331_000056952048_00234_22332_0000.N1
22333	SCI_NL__1PYDPA20060608_062406_000057342048_00235_22333_0000.N1
22334	SCI_NL__1PYDPA20060608_080442_000056942048_00236_22334_0000.N1
22335	SCI_NL__1PYDPA20060608_094518_000057342048_00237_22335_0000.N1
22336	SCI_NL__1PYDPA20060608_112554_000056942048_00238_22336_0000.N1
22337	SCI_NL__1PYDPA20060608_130630_000057342048_00239_22337_0000.N1
22338	SCI_NL__1PYDPA20060608_144705_000056952048_00240_22338_0000.N1
22339	SCI_NL__1PYDPA20060608_162741_000057342048_00241_22339_0000.N1
22340	SCI_NL__1PYDPA20060608_180817_000056952048_00242_22340_0000.N1
22341	SCI_NL__1PYDPA20060608_194853_000057342048_00243_22341_0000.N1
22342	SCI_NL__1PYDPA20060608_212929_000056942048_00244_22342_0000.N1
22343	SCI_NL__1PYDPA20060608_231005_000057342048_00245_22343_0000.N1
22416	SCI_NL__1PYDPA20060614_013340_000056952048_00318_22416_0000.N1
22417	SCI_NL__1PYDPA20060614_031416_000057352048_00319_22417_0000.N1
22418	SCI_NL__1PYDPA20060614_045452_000056952048_00320_22418_0000.N1
22419	SCI_NL__1PYDPA20060614_063528_000057352048_00321_22419_0000.N1
22420	SCI_NL__1PYDPA20060614_081604_000056952048_00322_22420_0000.N1
22421	SCI_NL__1PYDPA20060614_095640_000057352048_00323_22421_0000.N1
22422	SCI_NL__1PYDPA20060614_113716_000056952048_00324_22422_0000.N1
22423	SCI_NL__1PYDPA20060614_131751_000057352048_00325_22423_0000.N1
22424	SCI_NL__1PYDPA20060614_145827_000056952048_00326_22424_0000.N1
22425	SCI_NL__1PYDPA20060614_163903_000057352048_00327_22425_0000.N1
22426	SCI_NL__1PYDPA20060614_181939_000056952048_00328_22426_0000.N1
22427	SCI_NL__1PYDPA20060614_200015_000057352048_00329_22427_0000.N1
22428	SCI_NL__1PYDPA20060614_214051_000056952048_00330_22428_0000.N1
22429	SCI_NL__1PYDPA20060614_232127_000057352048_00331_22429_0000.N1
23246	SCI_NL__1PYDPA20060811_010646_000059902050_00146_23246_0000.N1
23247	SCI_NL__1PYDPA20060811_024721_000060042050_00147_23247_0000.N1
23248	SCI_NL__1PYDPA20060811_042759_000059902050_00148_23248_0000.N1
23249	SCI_NL__1PYDPA20060811_060834_000060042050_00149_23249_0000.N1
23250	SCI_NL__1PYDPA20060811_074912_000059902050_00150_23250_0000.N1
23251	SCI_NL__1PYDPA20060811_092947_000060042050_00151_23251_0000.N1
23252	SCI_NL__1PYDPA20060811_111024_000059902050_00152_23252_0000.N1
23253	SCI_NL__1PYDPA20060811_125059_000060042050_00153_23253_0000.N1
23254	SCI_NL__1PYDPA20060811_143137_000059902050_00154_23254_0000.N1
23255	SCI_NL__1PYDPA20060811_161212_000060042050_00155_23255_0000.N1

Orbit #	Level 1b Product
23256	SCI_NL__1PYDPA20060811_175250_000059902050_00156_23256_0000.N1
23257	SCI_NL__1PYDPA20060811_193325_000060042050_00157_23257_0000.N1
23258	SCI_NL__1PYDPA20060811_211402_000059902050_00158_23258_0000.N1
23361	SCI_NL__1PYDPA20060819_015541_000060042050_00261_23361_0000.N1
24149	SCI_NL__1PYDPA20061013_030746_000059972052_00047_24149_0000.N1
24150	SCI_NL__1PYDPA20061013_044906_000059482052_00048_24150_0000.N1
24151	SCI_NL__1PYDPA20061013_062859_000059962052_00049_24151_0000.N1
24152	SCI_NL__1PYDPA20061013_081019_000059482052_00050_24152_0000.N1
24153	SCI_NL__1PYDPA20061013_095012_000059962052_00051_24153_0000.N1
24154	SCI_NL__1PYDPA20061013_113132_000059482052_00052_24154_0000.N1
24155	SCI_NL__1PYDPA20061013_131124_000059962052_00053_24155_0000.N1
24156	SCI_NL__1PYDPA20061013_145245_000059482052_00054_24156_0000.N1
24157	SCI_NL__1PYDPA20061013_163237_000059972052_00055_24157_0000.N1
24158	SCI_NL__1PYDPA20061013_181358_000059482052_00056_24158_0000.N1
24159	SCI_NL__1PYDPA20061013_195350_000059962052_00057_24159_0000.N1
24160	SCI_NL__1PYDPA20061013_213511_000059482052_00058_24160_0000.N1
24356	SCI_NL__1PYDPA20061027_141120_000060242052_00254_24356_0000.N1
24874	SCI_NL__1PYDPA20061202_184137_000059912053_00271_24874_0000.N1
24992	SCI_NL__1PYDPA20061211_003228_000060022053_00389_24992_0000.N1
24993	SCI_NL__1PYDPA20061211_021315_000059912053_00390_24993_0000.N1
24994	SCI_NL__1PYDPA20061211_035340_000060032053_00391_24994_0000.N1
24995	SCI_NL__1PYDPA20061211_053427_000059912053_00392_24995_0000.N1
24996	SCI_NL__1PYDPA20061211_071452_000060022053_00393_24996_0000.N1
24997	SCI_NL__1PYDPA20061211_085540_000059912053_00394_24997_0000.N1
24998	SCI_NL__1PYDPA20061211_103605_000060022053_00395_24998_0000.N1
24999	SCI_NL__1PYDPA20061211_121652_000059912053_00396_24999_0000.N1
25000	SCI_NL__1PYDPA20061211_135717_000060032053_00397_25000_0000.N1
25001	SCI_NL__1PYDPA20061211_153804_000059912053_00398_25001_0000.N1
25002	SCI_NL__1PYDPA20061211_171829_000060032053_00399_25002_0000.N1
25003	SCI_NL__1PYDPA20061211_185916_000059912053_00400_25003_0000.N1
25004	SCI_NL__1PYDPA20061211_203941_000060022053_00401_25004_0000.N1
25331	SCI_NL__1PYDPA20070103_165509_000059912054_00227_25331_0000.N1
25414	SCI_NL__1PYDPA20070109_120441_000059922054_00310_25414_0000.N1
26176	SCI_NL__1PYDPA20070303_174059_000059862056_00070_26176_0000.N1
26411	SCI_NL__1PYDPA20070320_034214_000059912056_00305_26411_0000.N1
27221	SCI_NL__1PYDPA20070515_175210_000056972058_00113_27221_0000.N1
28094	SCI_NL__1PYDPA20070715_173353_000057522059_00485_28094_0000.N1
28982	SCI_NL__1PYDPA20070915_182114_000059922061_00371_28982_0000.N1

Orbit #	Level 1b Product
29855	SCI_NL__1PYDPA20071115_180453_000059602063_00242_29855_0000.N1
30399	SCI_NL__1PYDPA20071223_180949_000059922064_00285_30399_0000.N1
31258	SCI_NL__1PYDPA20080221_182435_000059592066_00142_31258_0000.N1
32102	SCI_NL__1PYDPA20080420_172928_000060232067_00485_32102_0000.N1
32961	SCI_NL__1PYDPA20080619_174750_000056972069_00342_32961_0000.N1
33805	SCI_NL__1PYDPA20080817_164920_000060042071_00184_33805_0000.N1
34664	SCI_NL__1PYDPA20081016_170345_000060042073_00041_34664_0000.N1
35907	SCI_NL__1PYDPA20090111_130744_000059912075_00282_35907_0000.N1
36430	SCI_NL__1PYDPA20090217_020131_000059792076_00304_36430_0000.N1
36825	SCI_NL__1PYDPA20090316_161746_000059912077_00198_36825_0000.N1
37207	SCI_NL__1PYDPA20090412_084634_000059832078_00079_37207_0000.N1
37717	SCI_NL__1PYDPA20090517_235159_000059962079_00088_37717_0000.N1
38200	SCI_NL__1PYDPA20090620_174456_000056932080_00070_38200_0000.N1
38510	SCI_NL__1PYDPA20090712_093047_000057112080_00380_38510_0000.N1
39016	SCI_NL__1PYDPA20090816_174933_000060042081_00385_39016_0000.N1
39437	SCI_NL__1PYDPA20090915_034135_000059922082_00305_39437_0000.N1
39813	SCI_NL__1PYDPA20091011_100659_000059962083_00180_39813_0000.N1
40312	SCI_NL__1PYDPA20091115_064627_000059602084_00178_40312_0000.N1
40740	SCI_NL__1PYDPA20091215_042144_000059922085_00105_40740_0000.N1
41112	SCI_NL__1PYDPA20100110_040429_000059912085_00477_41112_0000.N1
41612	SCI_NL__1PYDPA20100214_022404_000059392086_00476_41612_0000.N1
42012	SCI_NL__1PYDPA20100314_010320_000059912087_00375_42012_0000.N1
42494	SCI_NL__1PYDPA20100416_171223_000060032088_00356_42494_0000.N1
42908	SCI_NL__1PYDPA20100515_152025_000059962089_00269_42908_0000.N1
43350	SCI_NL__1PYDPA20100615_122840_000057362090_00210_43350_0000.N1
43778	SCI_NL__1PYDPA20100715_100513_000057132091_00137_43778_0000.N1
44220	SCI_NL__1PYDPA20100815_070609_000059612092_00078_44220_0000.N1
44660	SCI_NL__1PYDPA20100915_004859_000059932093_00017_44660_0000.N1
45092	SCI_NL__1PYDPA20101015_050736_000060072093_00449_45092_0000.N1
46361	SCI_NL__1PYDPA20110111_135149_000060133098_00226_46361_0000.N1
46886	SCI_NL__1PYDPA20110217_025504_000059583099_00320_46886_0000.N1
47282	SCI_NL__1PYDPA20110316_162715_000059693100_00285_47282_0000.N1
47665	SCI_NL__1PYDPA20110412_081716_000059383101_00237_47665_0000.N1
48177	SCI_NL__1PYDPA20110517_233608_000059743102_00318_48177_0000.N1
48662	SCI_NL__1PYDPA20110620_175305_000057023103_00372_48662_0000.N1
48973	SCI_NL__1PYDPA20110712_092547_000056743104_00252_48973_0000.N1
49481	SCI_NL__1PYDPA20110816_175947_000059593105_00329_49481_0000.N1
49903	SCI_NL__1PYDPA20110915_025744_000059713106_00320_49903_0000.N1

Orbit #	Level 1b Product
50281	SCI_NL__1PYDPA20111011_102641_000059263107_00267_50281_0000.N1
50782	SCI_NL__1PYDPA20111115_072233_000059623108_00337_50782_0000.N1
51211	SCI_NL__1PYDPA20111215_040220_000059813109_00335_51211_0000.N1
51605	SCI_NL__1PYDPA20120111_141347_000059813110_00298_51605_0000.N1
52129	SCI_NL__1PYDPA20120217_013535_000059573111_00391_52129_0000.N1
52396	SCI_NL__1PYDPA20120306_153756_000059253112_00227_52396_0000.N1

4 Task #1: Limb Cloud Algorithm Update

4.1 Introduction

The SCIAMACHY cloud detection algorithm (SCODA) is implemented in the SGP L1b-2 since Version 5.02 released in 2012. SCODA helps to discard cloud contaminated measurements during the limb profiles retrieval preventing spurious and erroneous results in the upper troposphere / lower stratosphere altitude region. Recently the scientific SCODA version maintained and developed at IUP-UB has been further reviewed and modified (see [R3]). The operational SCODA is updated accordingly.

The following modifications have been introduced into the SGP L1b-2 V7:

- lower colour index ratio (CIR) boundary for PSCs (now: **1.35** – in Northern Hemisphere and **1.3** – in Southern Hemisphere; previously: 1.35 for both Hemispheres);
- upper wavelength window for ice clouds (ICL) (now: **1683-1687** nm; previously: 1630-1634 nm)
- maximum (now: **28** km; previously: 25 km) and warning (now: **19** km; previously: 18 km) tangent heights (THs) for water clouds (WCL);
- maximum (now: **20** km; previously: 25 km) and warning (now: **19** km; previously: 18 km) tangent heights (THs) for ICL;
- maximum SZA (now: **89.9°**; previously: 88°);
- two new flags introduced for WCL: **4** - *partially cloudy, thick or multiple layers* and **5** - *fully cloudy, thick or multiple layers*;
- in case of multi-layered WCL the **highest** TH, where CIR exceeds lower CIR boundary, is taken as a cloud height (previously: the lowest one) as shown in Figure 4.1.

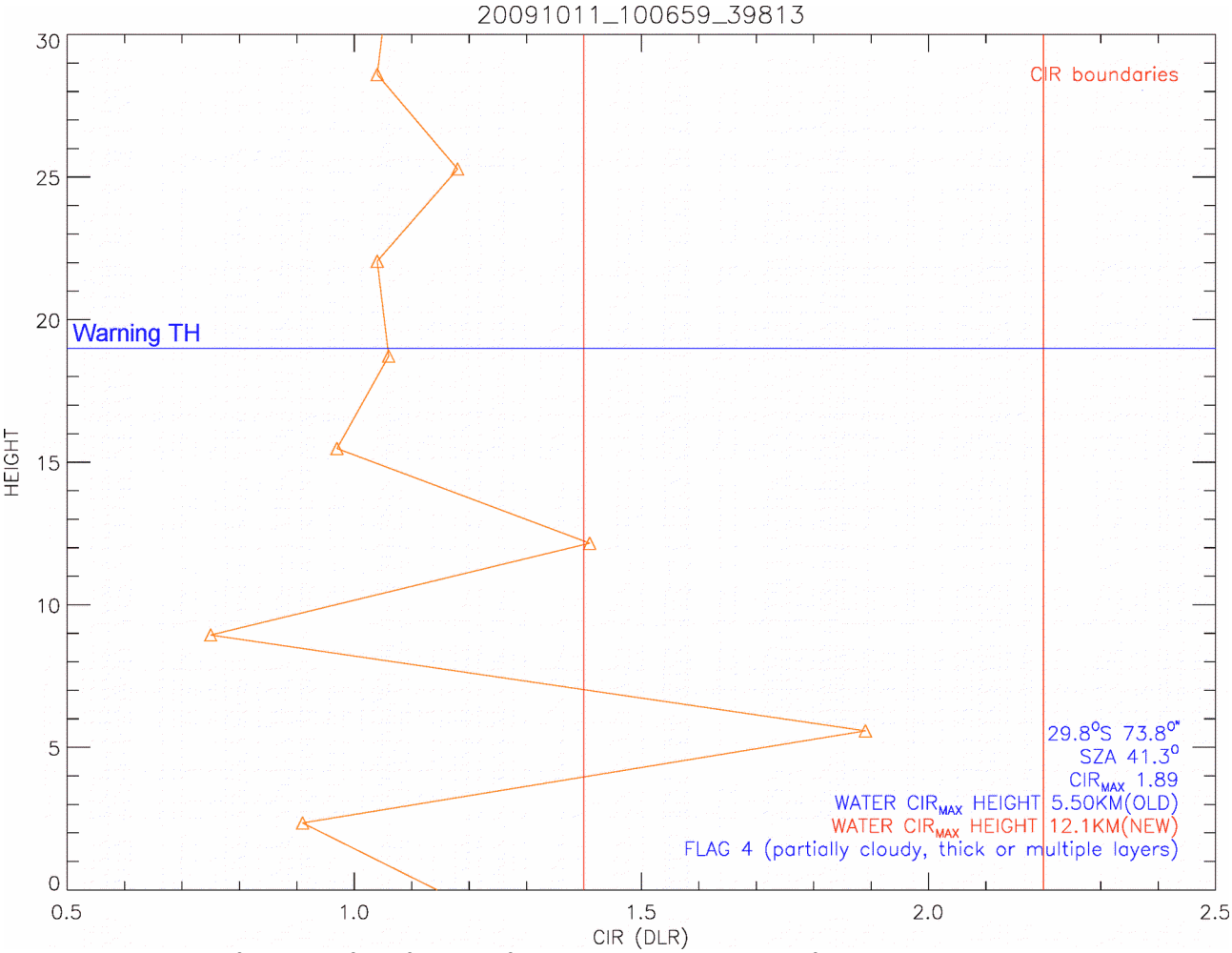

Figure 4.1: CIR as a function of TH for WCL for multilayer cloud. In the former SCODA version a cloud height was set to 5.5 km; in the latter 12.1 km.

4.2 Involved Partners

IUP-UB	K. U. Eichmann	Eichmann@iup.physik.uni-bremen.de
DLR-IMF	M. Meringer	Markus.Meringer@dlr.de
	S. Gretschany	Sergei.Gretschany@dlr.de

4.3 Verification Set-up

All product entries (cloud flags, heights, CIR_{MAX}) are compared.

4.4 Verification Data Set

See Table 3.1

4.5 Verification Results

Within the verification orbits there are 18859 matching records in the reference and the operational data sets. The reference data set was provided by the scientific algorithm developer IUP-UB. The scientific data set is of version 218 in the internal numbering.

For these records all relevant entries have been compared:

- cloud flags;
- maximum values of CIR (CIR_{MAX});
- height of CIR_{MAX}.

All above-listed parameters are retrieved for each cloud type: WCL, ICL and PSC.

An overview of an agreement of flags for all cloud types is presented in cross tables 4.1 - 4.3 below. For each flag combination the total number of occurrences as well as its relative fraction is given.

Table 4.1: Cross table for WCL flags. Flags meaning:

- *0 - no clouds*
- *1 - partially cloudy*
- *2 - partially cloudy & large CIR (>2.2)*
- *3 (9 at IUP) - bad data or cloud top height too heigh*
- *4 - partially cloudy, thick or multiple layers*
- *5 - partially cloudy, thick or multiple layers & large CIR (>2.2)*

	Flags IUP					
Flags DLR	0	1	2	9	4	5
0	1174(6.1%)	94(0.5%)	2	0	1	0
1	10(0.1%)	11263(58.9%)	217(1.1%)	0	117(0.6%)	0
2	0	2	4238(22.2%)	0	0	0
3	38(0.2%)	0	0	162(0.3%)	0	0
4	0	88(0.5%)	0	18(0.1%)	1785(9.3%)	5
5	0	0	4	0	0	33(0.2%)

Sum of non-diagonal elements: 3.1%, i.e. in 3.1% of the cases the results differ.

Table 4.2: Cross table for ICL flags. Flags meaning:

- *0 - water cloud*
- *1 - ice cloud*
- *2 - bad data (height of CIR_{MAX} is greater than the warning tangent height)*
- *3 (9 in IUP) - strange case (CIR_{MAX} is greater than the upper bound for the CIR)*

	Flags IUP			
Flags DLR	0	1	2	9
0	5206(27.3%)	500(2.6%)	0	0
1	412(2.2%)	12796(67.2%)	69(0.4%)	2
2	35(0.2%)	6	0	13(0.1%)
3	0	0	0	0

Sum of non-diagonal elements: 5.5%

Table 4.3: Cross table for PSC flags. Flags meaning:

- *0 – no PSC*
- *1 - PSC*

	Flags IUP	
Flags DLR	0	1
0	18825(98.4%)	10(0.1%)
1	1	300(1.5%)

Sum of non-diagonal elements: 0.1%.

4.5.1 Water clouds (WCL)

In Figure 4.2 CIR_{MAX} for WCL as a function of latitude is shown. The agreement of the scientific and the operational results is excellent: there are virtually no differences between them; for 99.96% of the records the difference is less than 0.1.

A scatter plot for WCL CIR_{MAX} as well as statistical parameters (Pearson coefficient, slope and intercept) are presented in Figure 4.3.

Finally, in Figure 4.4 a histogram of cloud heights (top panel) and a histogram of their differences (bottom panel) are shown. In the histogram of differences the relative number of occurrences for each bin is also indicated.

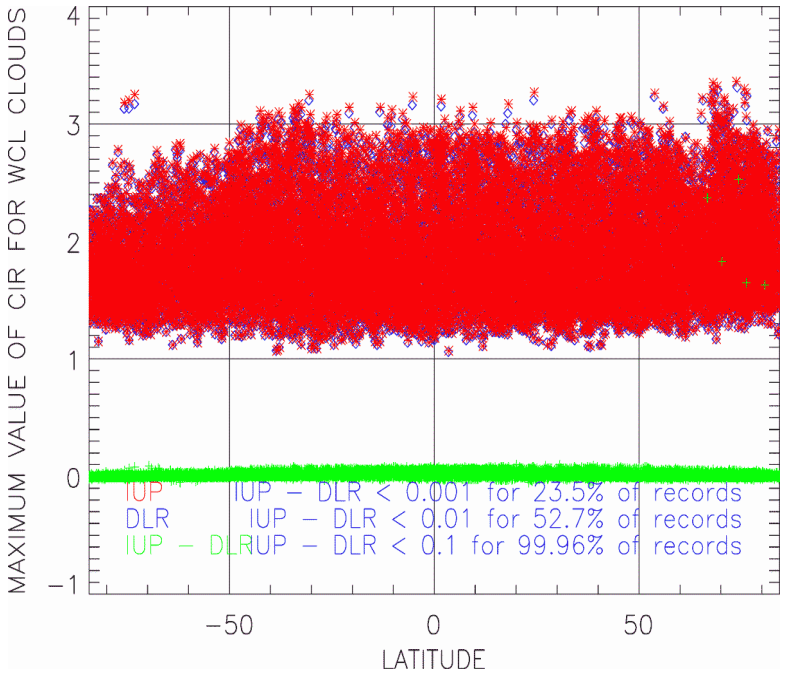

Figure 4.2: *CIR_{MAX} for WCL as a function of latitude. Both scientific and operational results are shown as well as a difference between them. For 99.96% of records the difference is less than 0.1.*

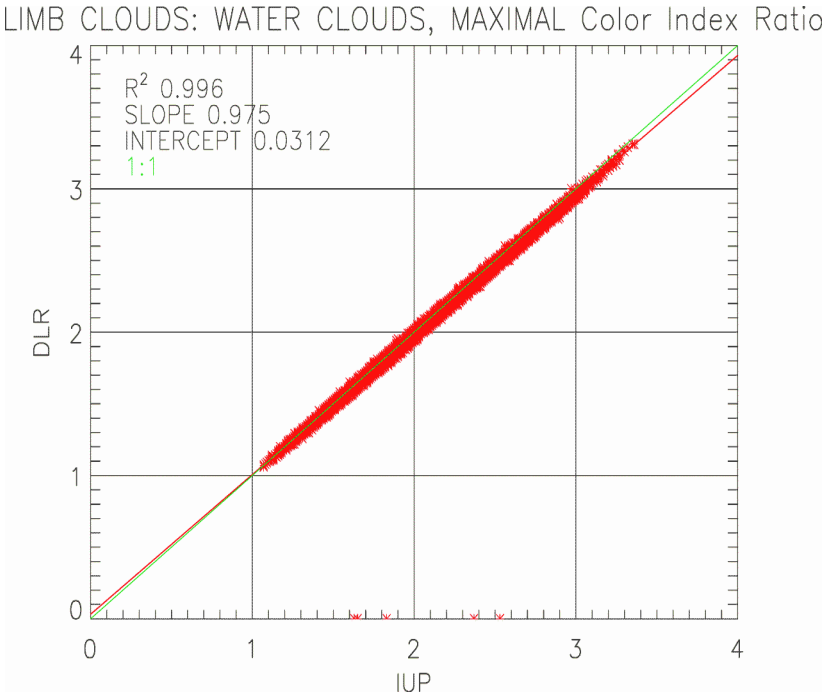

Figure 4.3: *Scatter plot for WCL CIR_{MAX}*

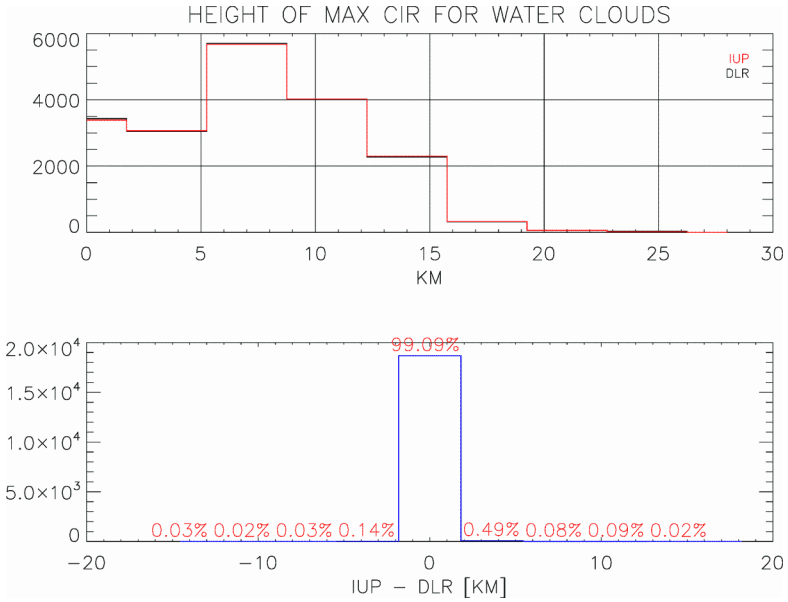

Figure 4.4: *Histogram of WCL cloud heights (top panel) and differences between scientific and operational cloud heights (bottom panel). Numbers in the bottom panel represent a relative fraction of occurrences for each bin of 3.5km width.*

4.5.2 Ice clouds (ICL)

In Figure 4.5 scientific and operational CIR_{MAX} for ICL are displayed as well as a difference between them.

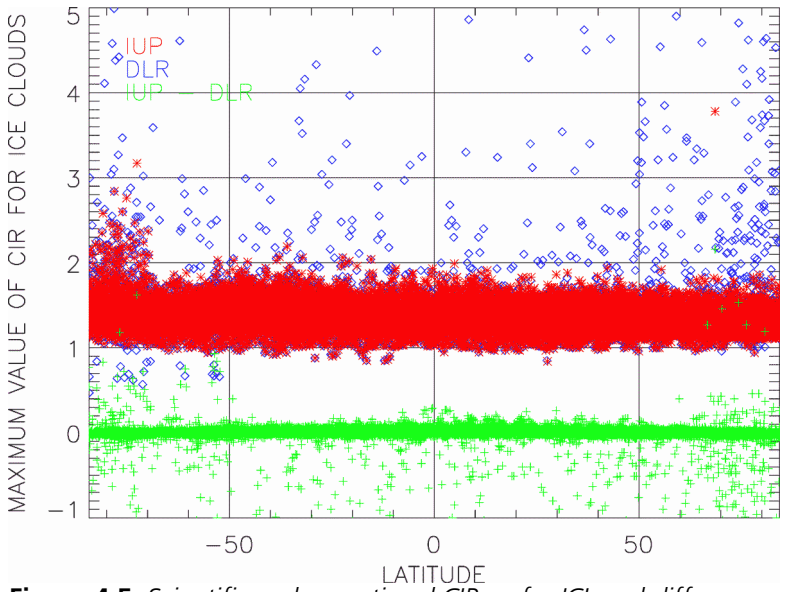

Figure 4.5: *Scientific and operational CIR_{MAX} for ICL and differences between them*

ICL detection is performed employing wavelength pair from infra-red band 1552/1685 nm. In this region SCIAMACHY suffers from numerous bad and dead pixels. In the scientific retrieval IUP-UB applies very strict filtering criteria to discard those pixels: pixels with very high negative and positive

radiances are filtered out, so that sometimes only 1-2 pixels remained. In the operational environment the dynamical bad and dead pixel mask provided by SRON is used. Discrepancies in bad and dead pixel classification lead to disagreement in ICL CIR_{MAX} for few records as seen in Figure 4.5. Nonetheless, for 23.8% of all records the difference is less than 0.001; for 52.3% less than 0.01; for 95.2% less than 0.1 and 98.7% less than 1.

In Figure 4.6 a scatter plot for ICL CIR_{MAX} is given.

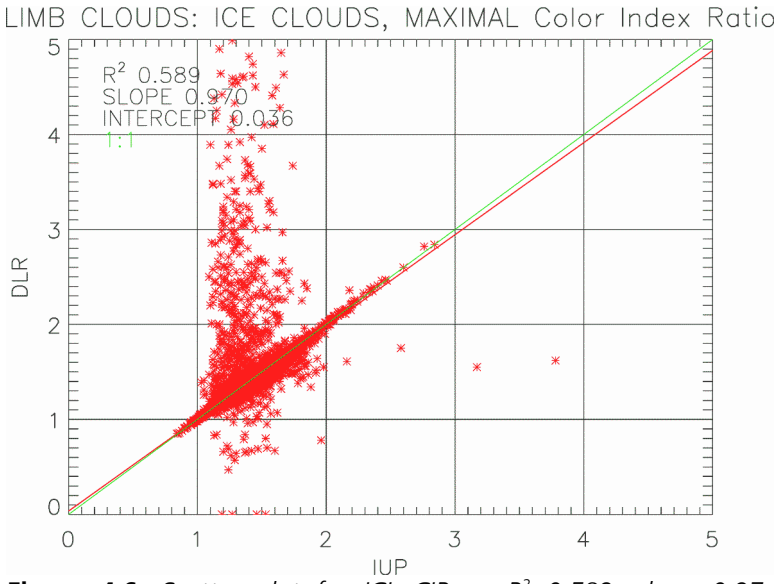

Figure 4.6: *Scatter plot for ICL CIR_{MAX}. R^2=0.589; slope=0.97; intercept=0.036.*

Scientific and operational ICL cloud heights demonstrate a very good agreement: 95.7% of all records has the same cloud height (see Figure 4.7).

4.5.3 Polar stratospheric clouds (PSC)

PSC is a quite rare phenomenon. They are encountered only in the winter polar stratosphere. In the verification data set only 311 (from 18859) records are characterized by presence of PSC (either in the scientific or in the operational data set). In 300 cases PSCs are detected by both algorithms; in 10 cases "scientific" PSCs were not detected by the operational processor and in 1 case it was vice versa (see Table 4.3).

Comparing PSC CIR_{MAX} the following statistic emerges: for 89 records (28.6%) the difference between the scientific and the operational CIR_{MAX} is less than 0.001; for 211 records (67.8%) it is less than 0.01; for 299 (96.1%) less than 0.1.

A scatter plot for PSC CIR_{MAX} demonstrates an excellent agreement for this entry (see Figure 4.8).

If PSC is detected by both the scientific and the operational algorithms, then the retrieved cloud height is also the same (in 298 cases or 99.3%, see Figure 4.8). In 2 cases the operational PSC cloud height differs from the scientific one by one tangent height step: operational 24.6 km – scientific 21.4 km and operational 18.3 km – scientific 15 km.

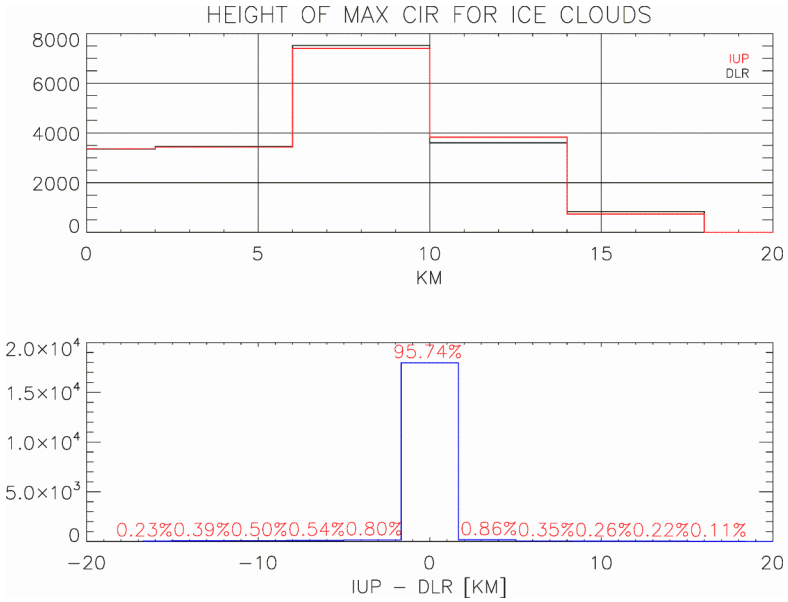

Figure 4.7: *Histogram of ICL cloud heights (top) and differences between scientific and operational results (bottom)*

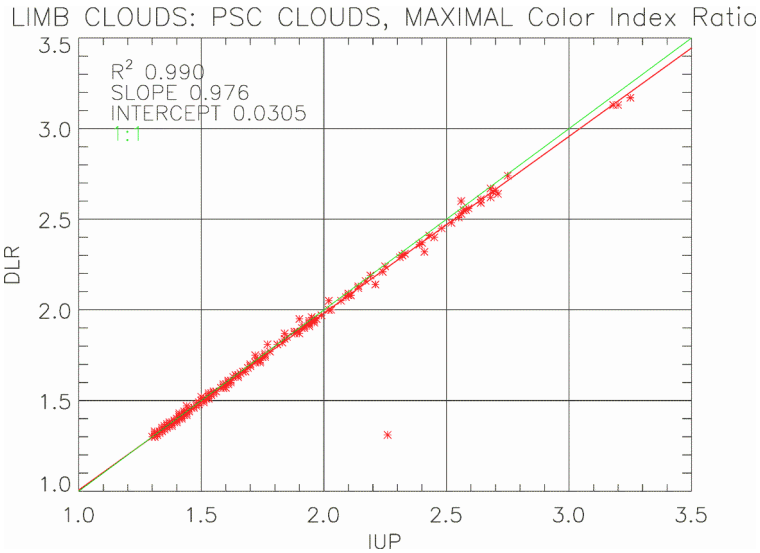

Figure 4.8: *Scatter plot for PSC CIR_{MAX}*

5 Task #2: Tropospheric BrO

5.1 Introduction

In addition to the BrO total columns that are part of the operational product, the current SGP version 7 performs also a separation of the total columns in a tropospheric and a stratospheric part. The BrO tropospheric columns are a new product. The scientific algorithm has been developed at BIRA. The verification of the new product is done by comparison with the BIRA scientific product.

5.2 Involved Partners

BIRA	N. Theys	Nicolas.Theys@aeronomie.be
DLR	M. Meringer	Markus.Meringer@dlr.de
	S. Gretschany	Sergei.Gretschany@dlr.de

5.3 Verification Set-up

The main result of both data sets – VCD_{TROPO} – is compared. Other intermediate results are checked if necessary.

5.4 Verification Data Set

See Table 3.1.

5.5 Verification Results

In Figure 5.1 (a, b) the absolute and relative differences between the scientific BIRA product and the operational results are shown in form of histograms. There is practically no bias between the two datasets. Average difference is less than $1x10^{12}$ molec x cm^{-2} or less than 7%. The error analysis of the retrieval made in [R4] estimated the error to be around $1x10^{13}$ molec cm^{-2}.

The scatter plot for the operational and the reference data is in Figure 5.1 (c). The correlation coefficient is very good (0.913); slope is 0.97, close to ideal; intercept is $-5.72x10^{11}$ molec x cm^{-2} in line with the average difference shown in the histogram (a).

During the implementation phase it has been discovered that there is a small time trend in the operational results, which is not to be expected. To overcome this drawback an equatorial correction has been suggested by BIRA and implemented into the operational environment. All SCDs (from all orbits of this day) in the equatorial latitudinal band (5°S-5°N) are averaged and then subtracted from all SCDs. Then a constant SCD value of $7.5x10^{13}$ molec x cm^2 is added to compensate for the equatorial value. By doing so, any constant offset is automatically removed as can be seen in Figure 5.1 (d), where slopes and intercepts of a linear fit function for each orbit of the verification data set are plotted. Apart from few exceptions the slopes are in a range between 0.9 and 1 and the intercepts between $-5x10^{12}$ and $5x10^{12}$ molec x cm^2.

Despite all efforts one small issue in the operational processor remained unsolved. In cases when cloud heights coincide with the assumed bulk of the tropospheric BrO (4km<CTH<6km) operational AMF_{TROPO} is systematically larger than the scientific one (see Figure 5.2 (a)). It has to be noted that only pixels with low cloud

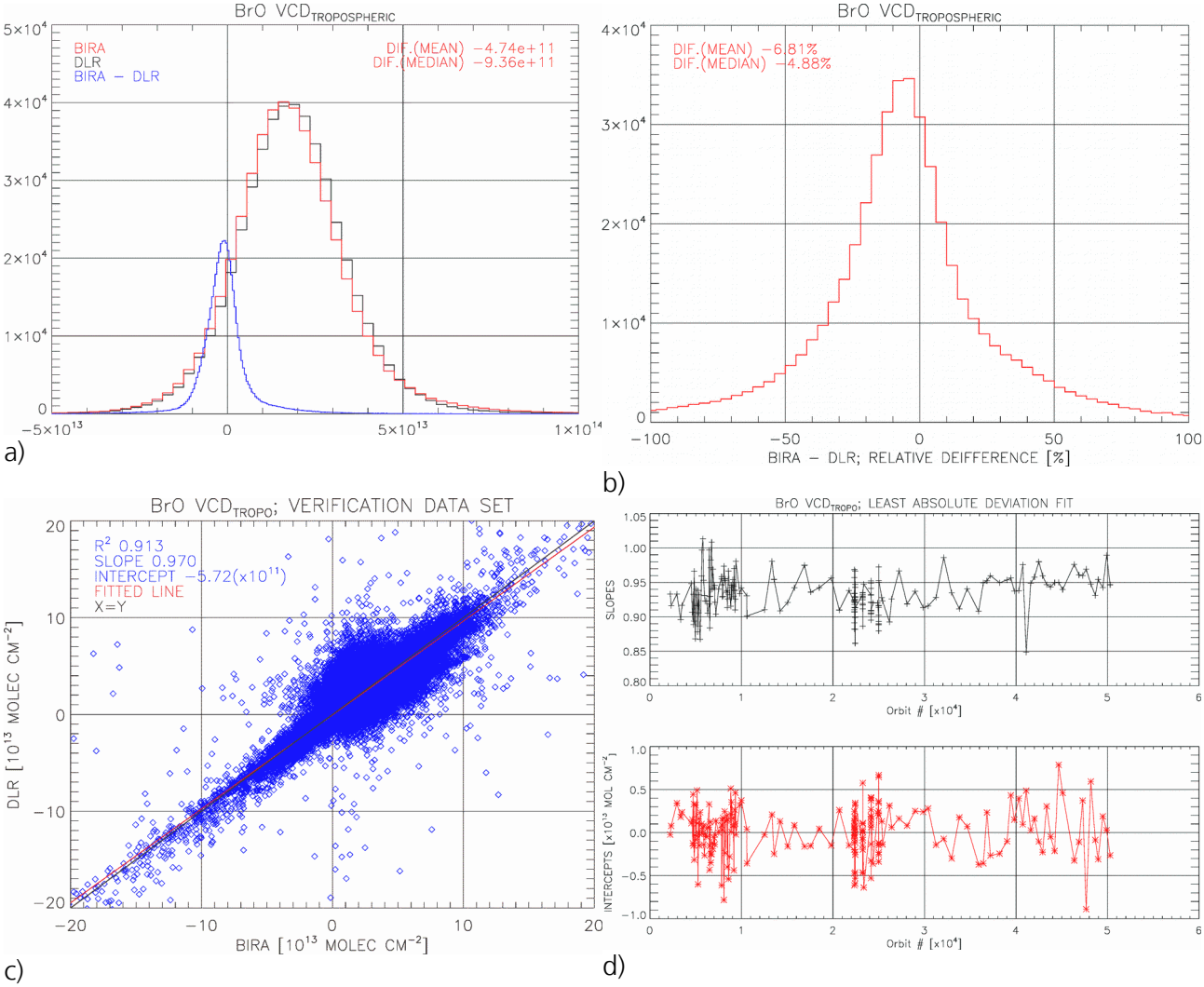

Figure 5.1: *Histograms of absolute (a) and relative (b) differences between scientific BIRA and operational BrOtropo products. The scatter plot for two data sets is shown in panel (c). Panel (d) shows slopes and intercepts of the linear fit function for each orbit.*

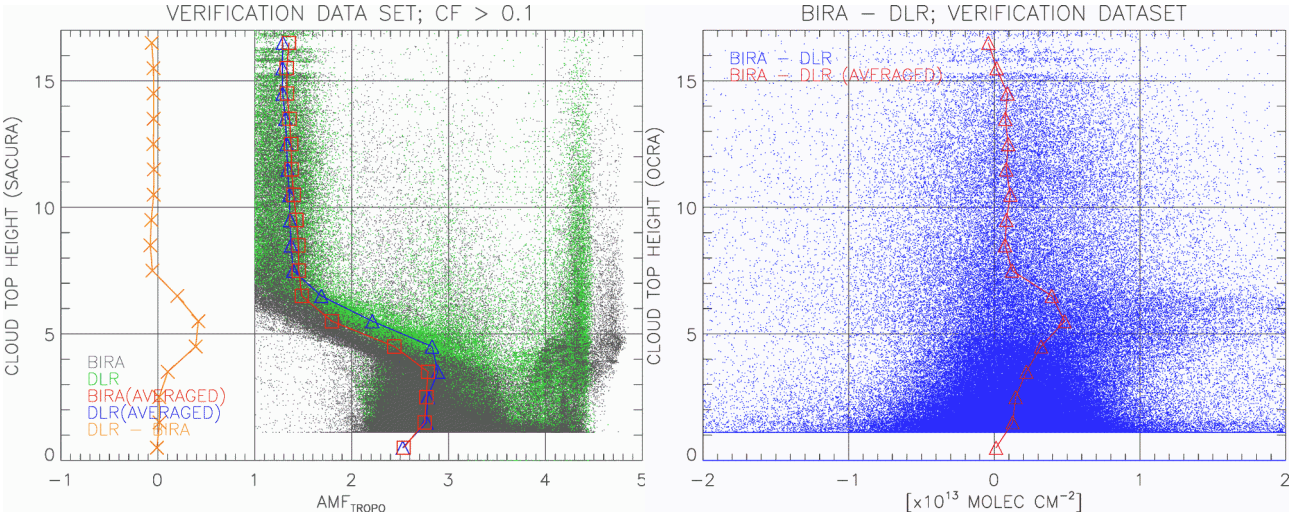

a) b)

Figure 5.2: *AMFtropo as a function of cloud top height (a). Difference between the scientific and operational results as a function of cloud top height (b).*

coverage (CF<0.4) are placed in the operational product and considered for the verification. Among all pixels only 5.5% has CTH between 4 and 6 km and affected. For these pixels BrO_{TROPO} is underestimated by 4-5x10^{12} molec x cm^2 (~20%) as compared to BIRA.

Summarizing, average difference between the operational and the reference data sets is less than 1x10^{12} molec x cm^2. In cases when clouds are between 4 and 6km (the peak height of the assumed tropospheric BrO profile) the differences could be larger (up to 4-5x10^{12} molec x cm^2), operational BrO_{TROPO} being underestimated. However, only 5.5% of pixels are affected. But even in these cases discrepancy between two datasets is below the estimated error for this product (1x10^{13} molec cm^{-2}). Taking all this into account, the verification of BrO_{TROPO} product can be considered as successful.

6 Regression Test

After all major L1b-2 processor updates had been implemented, debugged and checked, the regression test was performed in order to check whether any side effects appeared in the processor and if L2 products were negatively affected. In the regression test the L2 processor versions with (V. 7) and without (V. 6.01) the latest changes have been compared. The regression test is limited to products with *unchanged* retrieval code.

In the test all product entries have been compared[1].

The discrepancies between two versions are listed and explained below.

- **CHOCHO:** differences due to numerical problems when calculating AMF. To calculate AMF, LIDORT takes a logarithm of ratio of two intensities with and without CHOCHO. Since CHOCHO is a very weak absorber, these two numbers are usually very close, leading to their ratio being very close to unity and, consequently, the logarithm of it very close to zero. During these operations possible numerical discrepancies are being propagated towards more significant digits. For example, if intensity with CHOCHO differs in the 16th significant digit (marked **bold red**) in two independent runs:
  - IPA1 = 0.0989944914970179**7**23
  - IPA2 = 0.0989944914970179**4**46

  and intensity without CHOCHO is equal (IPANG = 0.0989944914999901365), the logarithm of their ratio is:
  - log(IPANG/IPA1))=3.0023**5**392098824797e-11 in the first case and
  - log(IPANG/IPA2))=3.0023**7**612544873983e-11 in the second.

  As is clearly seen the discrepancy between these two results is in a more significant position.The problem roots not in the wrong implementation into the processor, but in the compiler.
- **tropospheric NO_2:** Bug-fix after v6.01 (false tropopause height for NO_2 limb profile integration). This bug-fix leads to a small improvement of the operational results as compared to the scientific reference algorithm (Figure 4.1);
- **limb NO2 and BrO:** in rare cases limb cloud heights have changed due to the new SCODA version. This affected both NO2 and BrO profiles. Ozone profiles remain unchanged;
- **Discrepancies for Orbits 50782 and 51211:** the identification of processable states has been improved (previously simply the measurement category group was used, which e.g. also identified limb mesosphere measurements as processable). Due to this update there are 5 less processable states for both orbits in the V7 L2 products.

1 Note that all test up to here are done with Level 1 V8 as input.

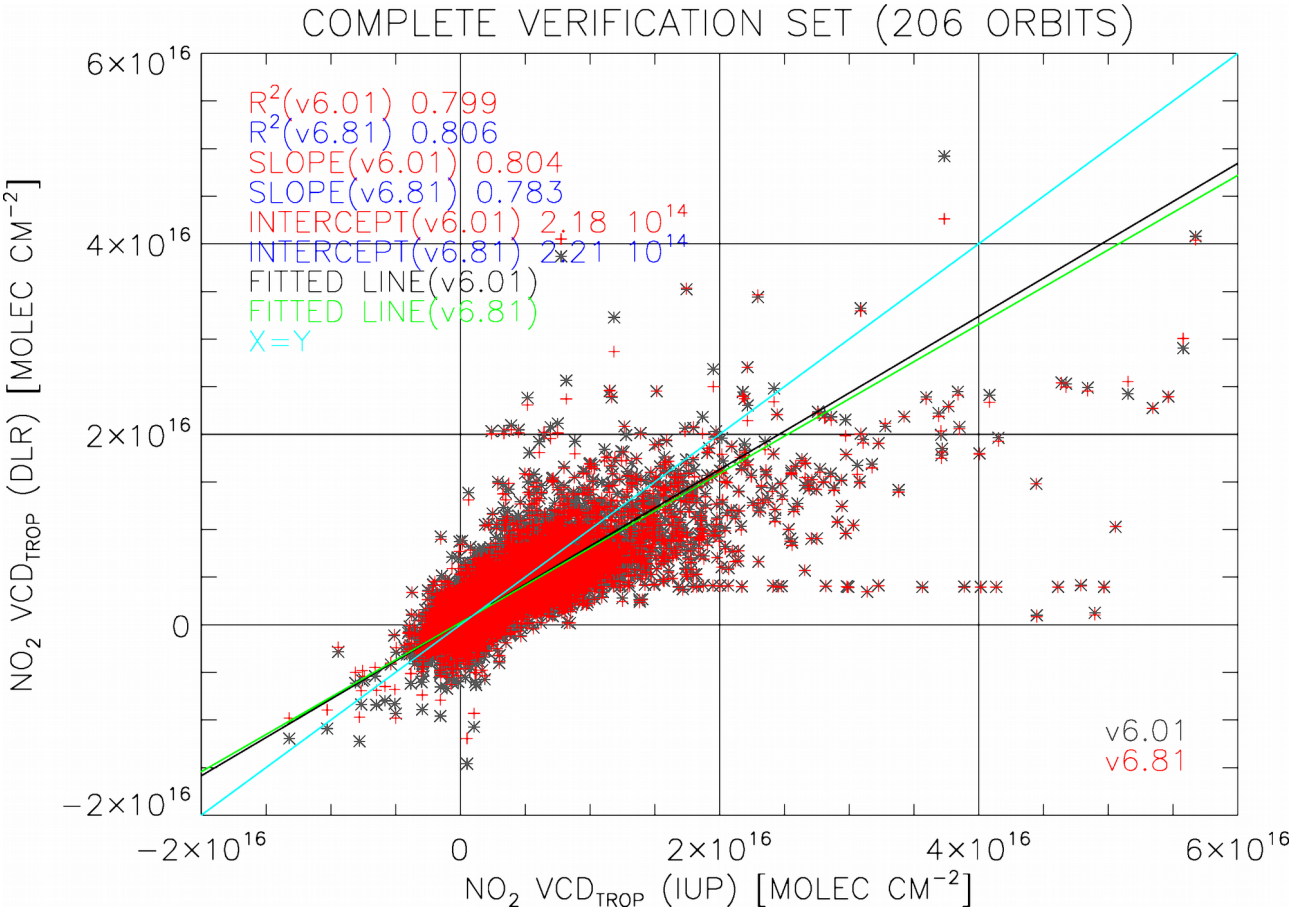

Figure 6.1: *Scatter plot for the operational (v6.01 and v7) and the scientific (IUP) tropospheric NO2 VCDs.*

7 Step 2 Verification Nadir UV/VIS Trace Gases

7.1 Total Column O_3

7.1.1 Operational Algorithm

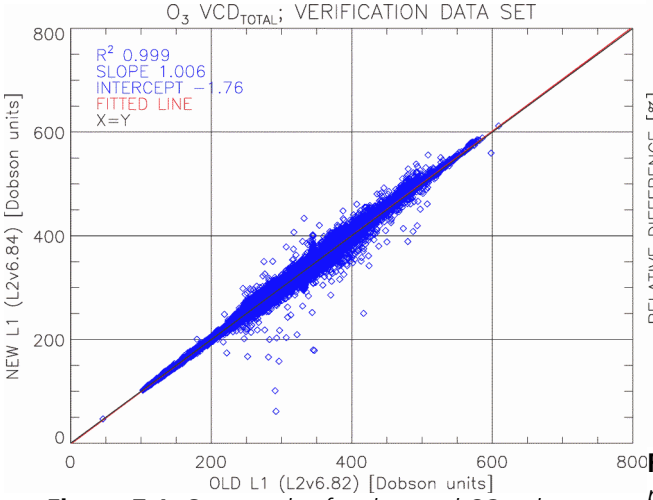

Figure 7.1: *Scatter plot for the total O3 columns*

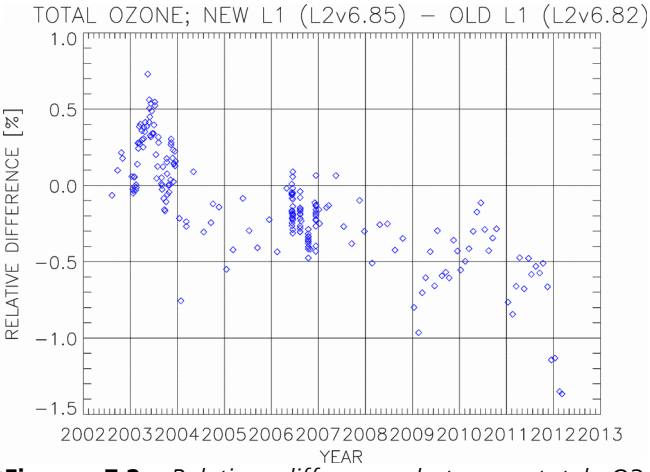

Figure 7.2: *Relative difference between total O3 product retrieved using L1v9 and L1v8 as a function of time*

There is an excellent agreement between total ozone columns retrieved from L1v9 and L1v8. However, it has to be noted that there appears to be a small negative difference of ca. 1% for the entire mission duration. Looking at the individual VCDs generated using Level 1 V8 and Level1 V9, no clear ttrned in either data set couldb be identified (Figure 7.3 - Figure 7.5). The absolute difference between the 2 VCDs does not show a clear trend (Figure 7.6). If one can draw conclusions from the limited dataset, one can maybe identify 3 steps in the curve and an increase towards the last data points,

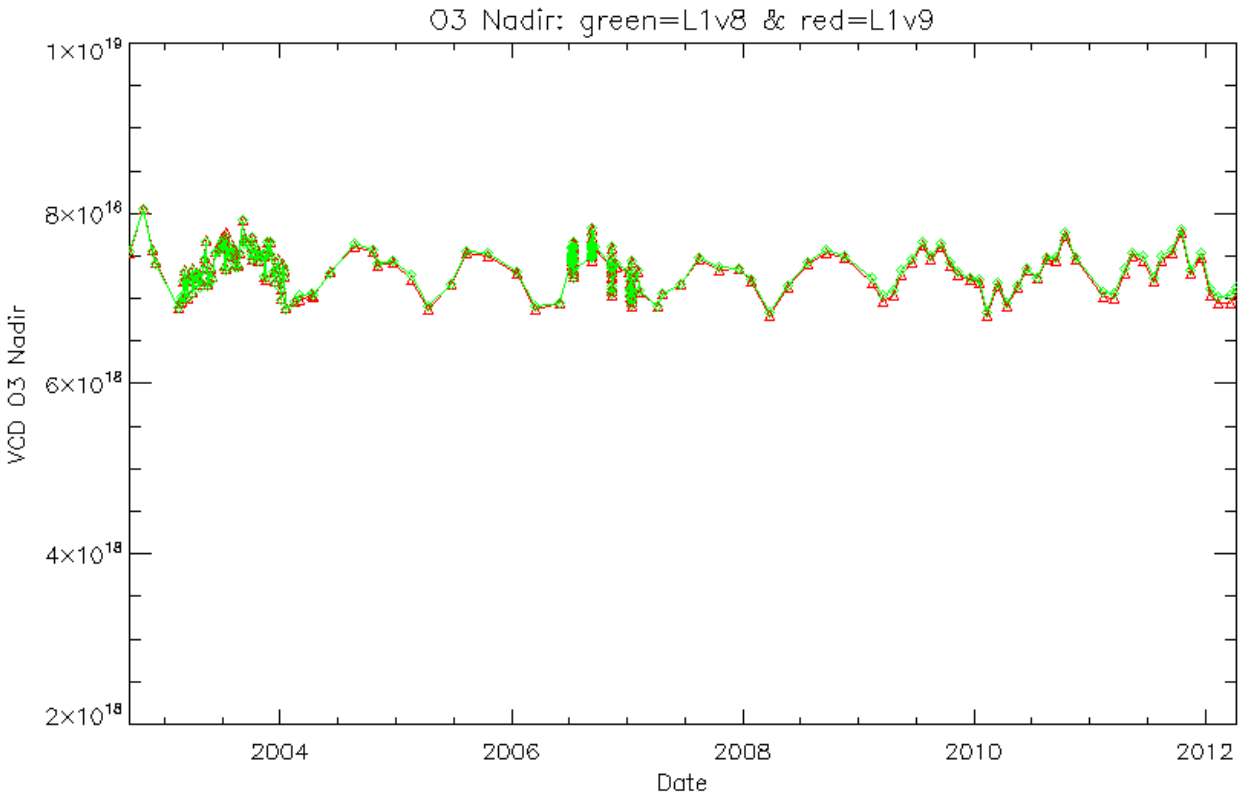

Figure 7.3: *The VCD (molec/cm^2) of O3 as a function of time. The green curve (reference) is obtained from Level 1 v8 and the red one if from Level 1v9.*

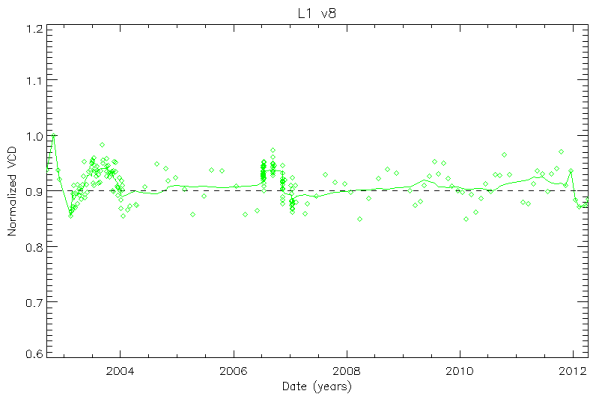

Figure 7.4: *Normalized VCD of O3 obtained from Level 1 v8 as a function of time in years. The continuous curve is the smoothed one.*

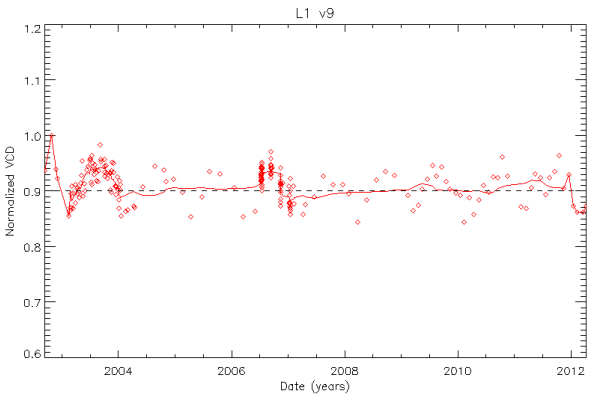

Figure 7.5: *Normalized VCD of O3 obtained from Level 1 v9 as a function of time in years.*

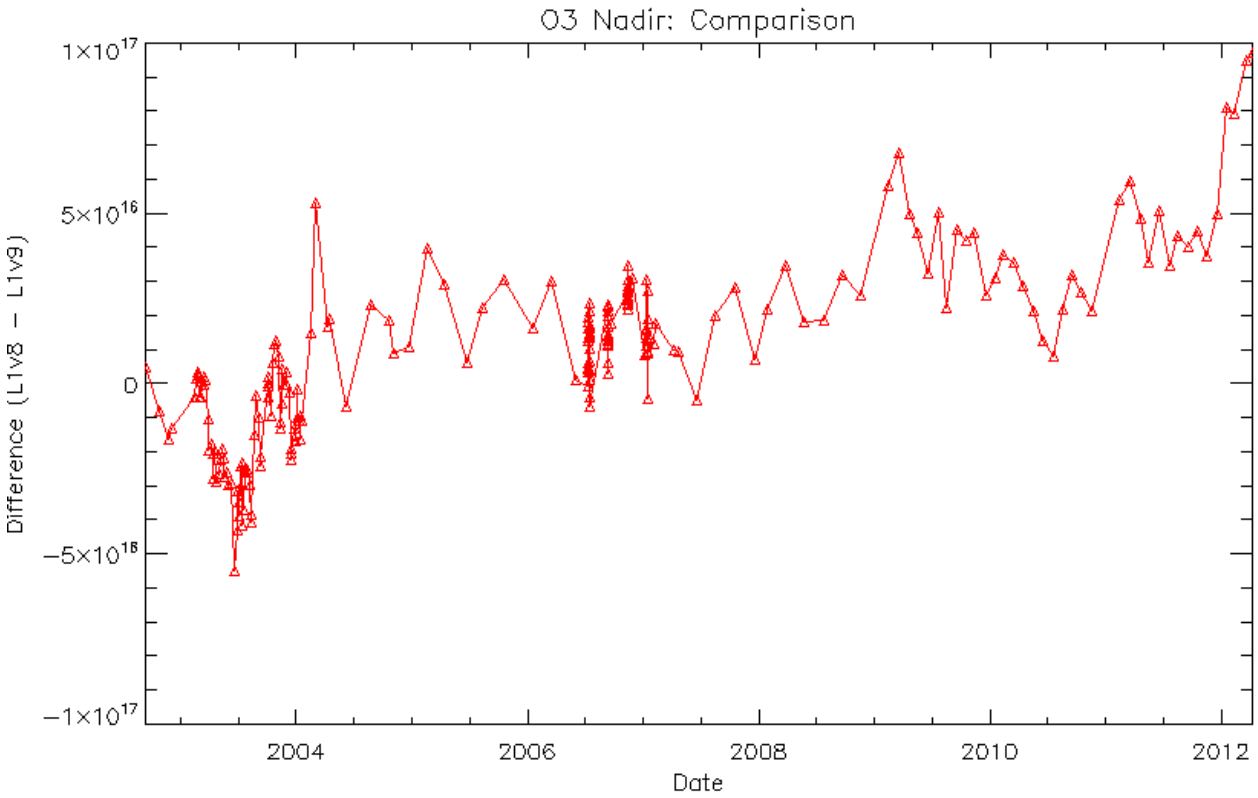

Figure 7.6: *O3 Nadir: Difference between the two Level 2 versions from L1v8 and L1v9.*

A comparison of the radiances for the O3 retrieval window shows that the radiances in Level 1 version 9 are systematically higher than those of version 8 (see Figure 7.7). We also looked at arbitrarily picked ratios of radiances between radiances for version 8 and version 9. The overall change over time is not systematic, but the change in the spectral domain seems to increase with time: the blue end of the spectrum shows a higher ratio than the red end (see Figure 7.8). However, this could just be effect caused by the random selection of the 6 spectra.

A conclusive result can only be reached after validation and the analysis of the whole mission dataset. The differences give no reason to change the algorithm at this point in time and the verification can be regarded as successful.

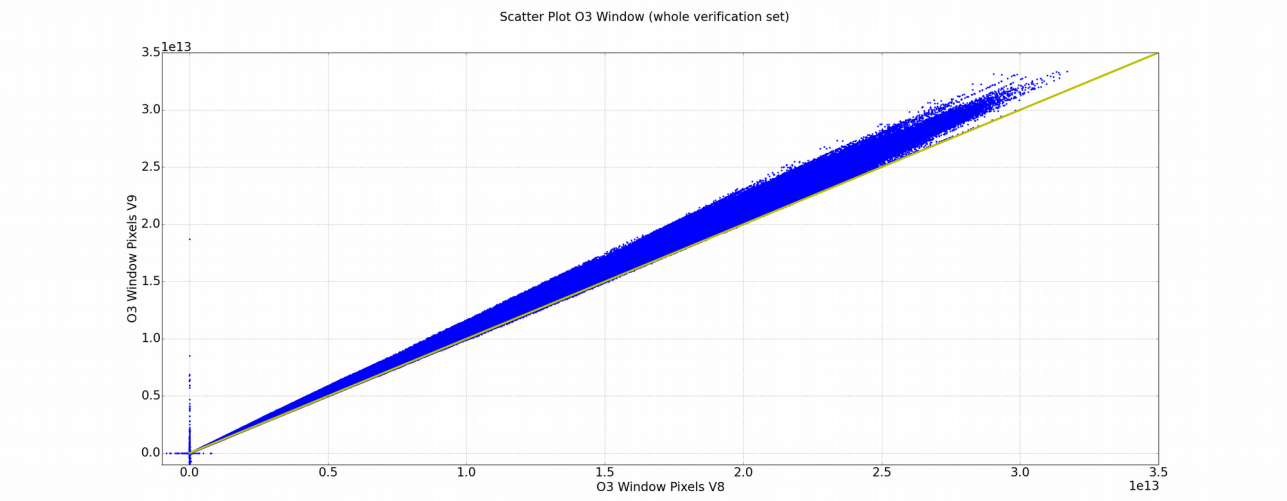

Figure 7.7: *Scatter plot of radiances in the O3 retrieval window: x-axis V8 and y-axis V9 processor. The radiances for version 9 are systematically higher. The yellow line is the 1-1 line.*

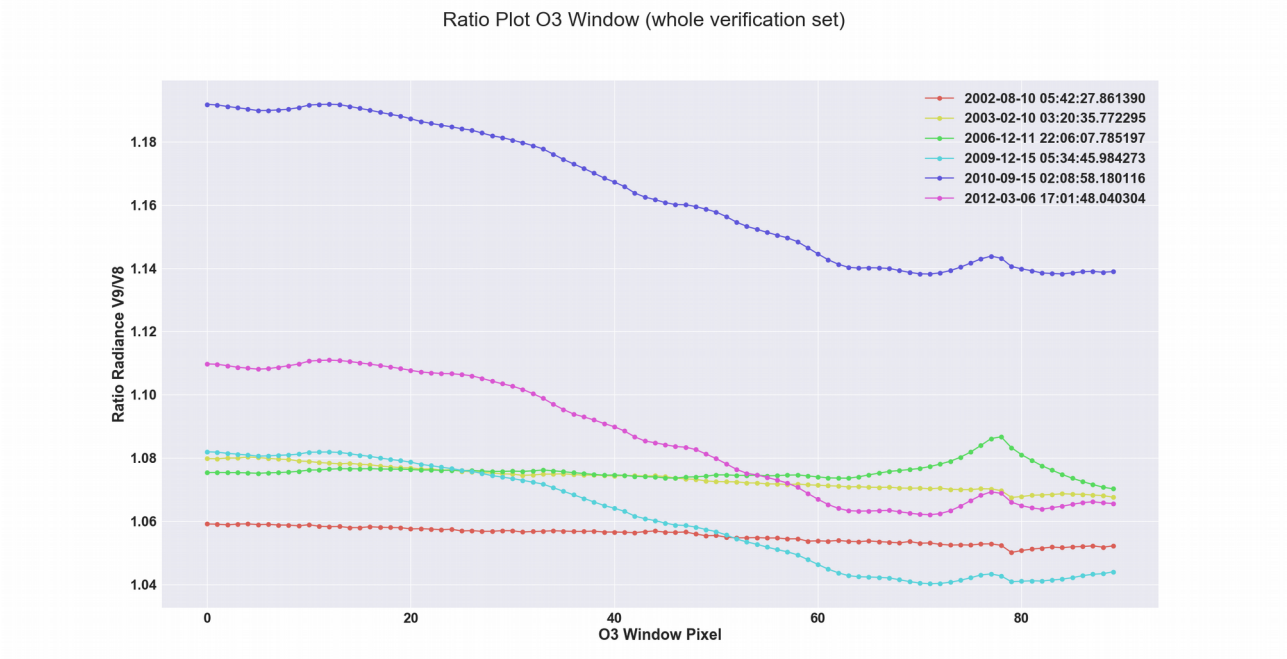

Figure 7.8: *Ratio of radiances (Level 1 V9/Level 1 V8) in the O3 retrieval window for 6 arbitrarily picked spetcra.*

7.2 Total Column NO_2

7.2.1 Operational Algorithm

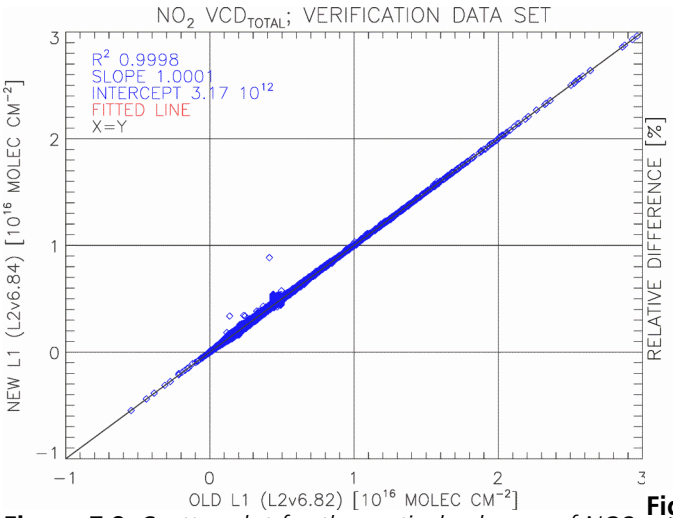

Figure 7.9: *Scatter plot for the vertical columns of NO2*

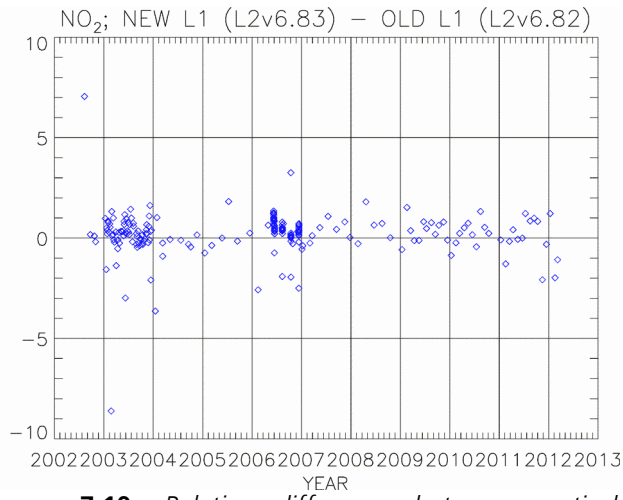

Figure 7.10: *Relative difference between vertical columns of NO2 retrieved using L1v9 and L1v8 as a function of time*

Transition from the old to newer L1 versions caused practically no impact on NO2 VCDs. Relative differences between two product versions are mostly well within 2% without any time drifting.

7.3 Total Column BrO

7.3.1 Operational Algorithm

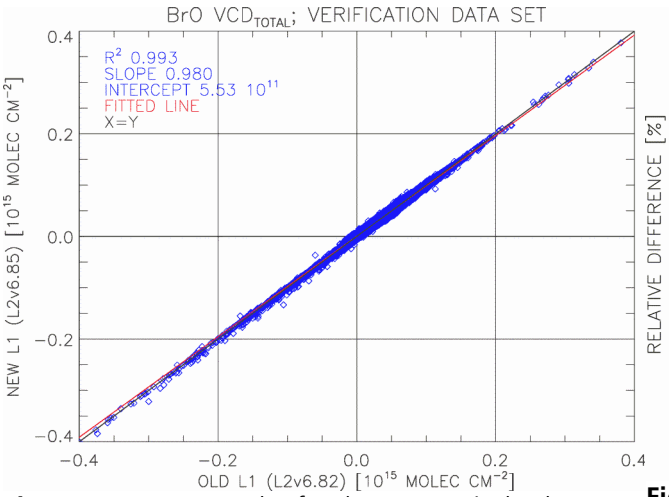

Figure 7.11: *Scatter plot for the BrO vertical columns*

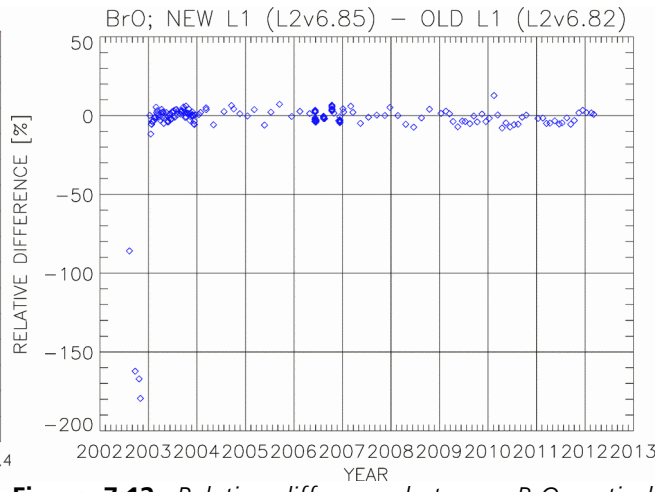

Figure 7.12: *Relative difference between BrO vertical columns retrieved using L1v9 and L1v8 as a function of time*

For the verification orbits from Year 2002 very noticeable differences between two data sets are found. The BrO VCDs processed using the new L1v9 are significantly lower than the ones from the

previous version. Apart from this issue no further shortcomings are observed when using the newer L1 version. The low values in 2002 can be explained by the missing proper A0 sun mean reference in the calibration database. When the calculations for this report where done, the A0 measurements that were done with the wrong mirror position were not yet exchanged with a static, valid one from December 2012.

7.4 Total Column HCHO

7.4.1 Operational Algorithm

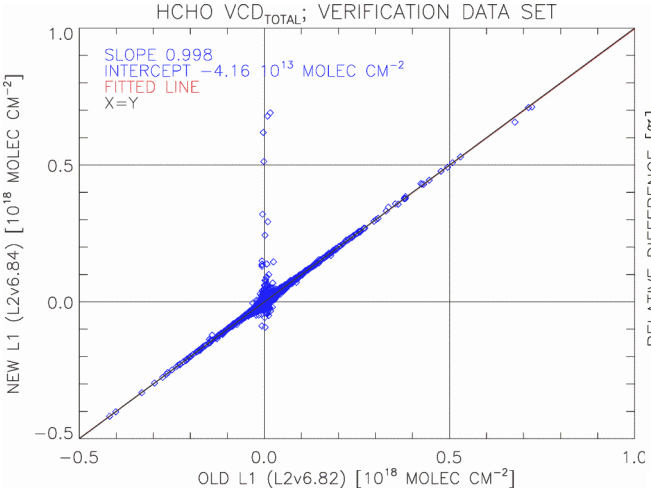

Figure 7.13: *Scatter plot for the HCHO vertical columns*

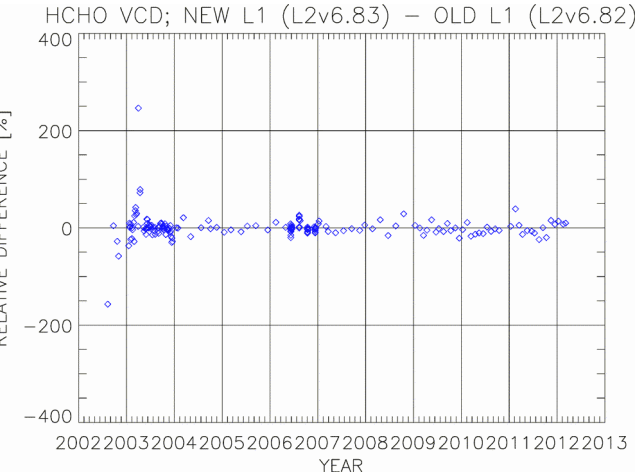

Figure 7.14: *Relative difference between HCHO vertical columns retrieved using L1v9 and L1v8 as a function of time*

Scatter plot for the formaldehyde VCDs retrieved from the L1v8 and L1v9 is shown in Figure 7.13. The figure demonstrates a very good agreement between the two data sets. Relative differences between two versions of formaldehyde product are within 20% for a predominant majority of orbits, which is fully acceptable considering low absolute values of HCHO VCDs. For the 2002 values the same remark as for BrO applies: the A0 SMRs were not exchanged in the calibration database.

7.5 Total Column SO_2

7.5.1 Operational Algorithm

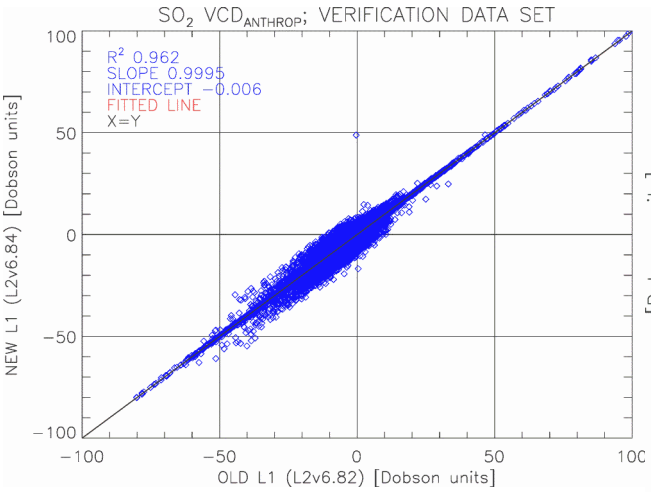

Figure 7.15: *Scatter plot for the (anthropogenic) SO2 vertical columns*

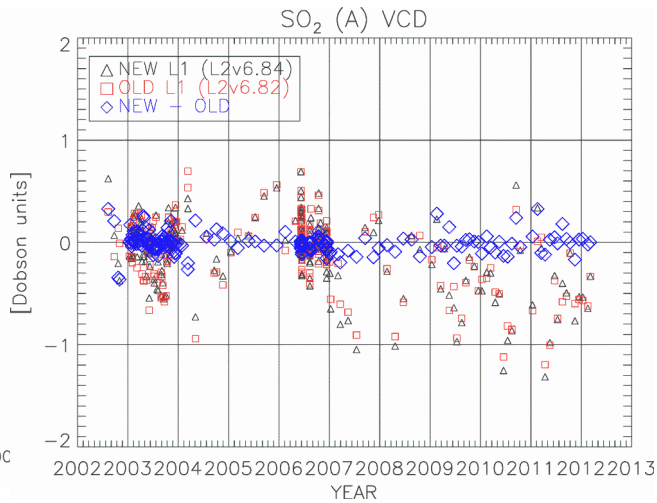

Figure 7.16: *Medians of anthropogenic SO2 VCDs retrieved using L1v9 and L1v8 for each orbit as well as absolute differences between them as a function of time*

The comparison of the SO_2 VCDs retrieved from the L1v8 and L1v9 is shown in Figures 7.15 and 7.16. Only results for the anthropogenic SO_2 are shown. The volcanic SO_2 behaves in a very similar way.

No issues have been found in the SO2 data retrieved from the L1v9.

7.6 Slant Column OClO

7.6.1 Operational Algorithm

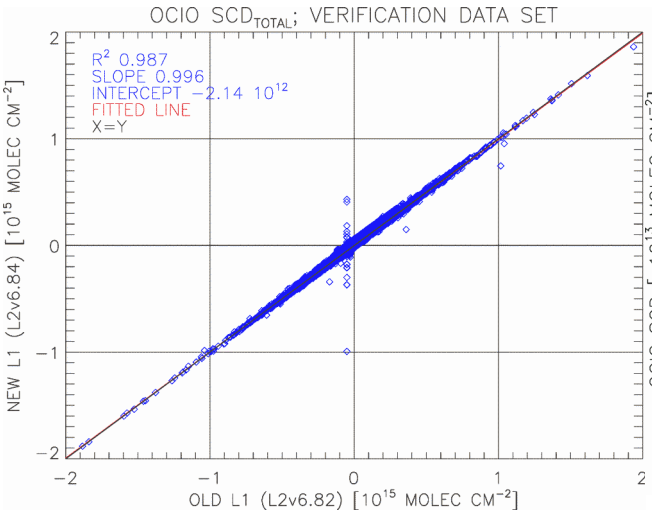

Figure 7.17: *Scatter plot for the OClO slant columns*

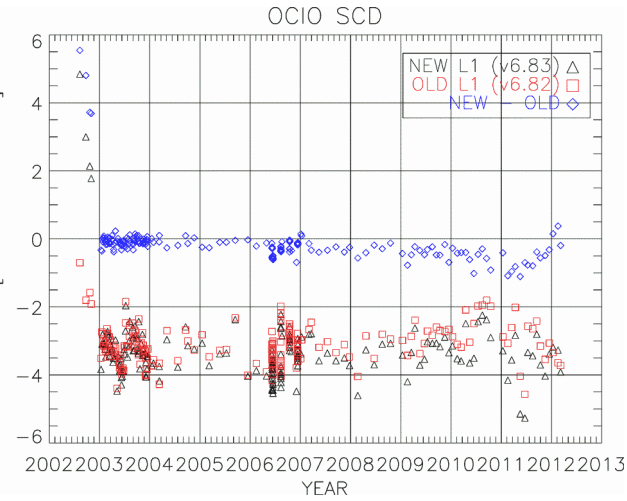

Figure 7.18: *Medians of OClO SCDs retrieved using L1v9 and L1v8 for each orbit as well as absolute differences between them as a function of time*

The fitting window for the OClO retrieval is 365 -389 nm, which is very near to the fitting window for BrO. So the OClO results for the Year 2002 are also affected in a similar way as BrO total columns. The scatter plot for the whole verification data set is shown in Figure 7.17. It has to be noted that measurable quantities of OClO are only present in the polar regions in twilight conditions. In the tropics and low latitudes the algorithm suffers from biases and retrieves negative results. This influences the medians taken over the whole orbit (and consequently also all latitudes) as seen in Figure 7.18, which show negative values.

Apart from the orbits from 2002 the agreement for the rest of the verification data set is very good.

7.7 Total Column H_2O

7.7.1 Operational Algorithm

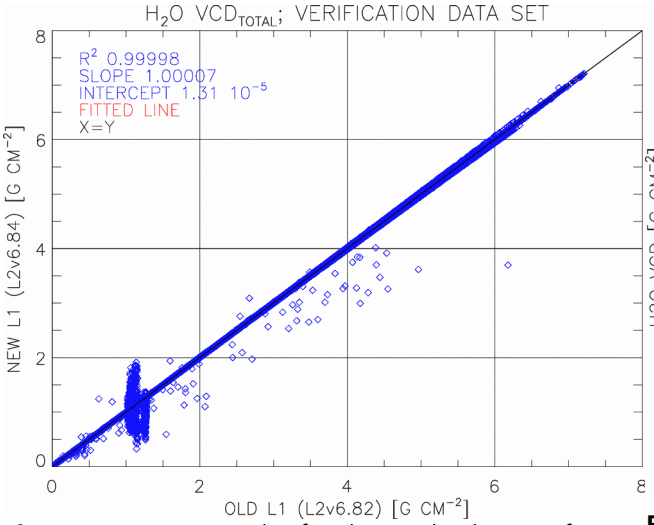

Figure 7.19: *Scatter plot for the total columns of water vapour*

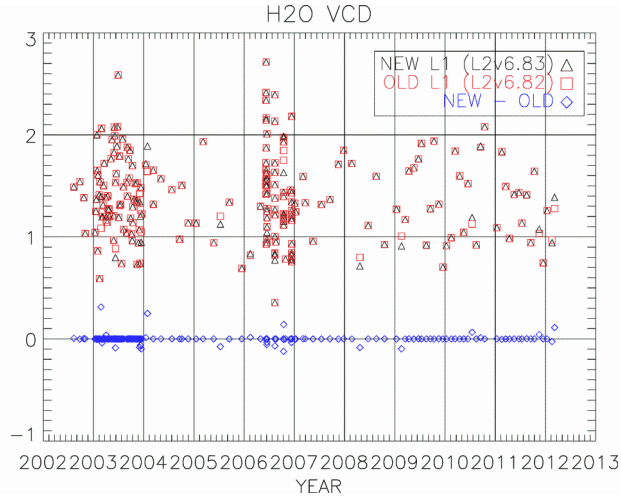

Figure 7.20: *Medians of total columns of H2O retrieved using L1v9 and L1v8 for each orbit as well as absolute differences between them as a function of time*

The results of the L1v8 – v9 comparison are shown in Figures 7.19 and 7.20. The agreement is excellent. The deviation of the two data sets is in the order of the expected precision of the retrieval (maximum about +-0.2 g/cm 2, typical values < 0.05 g/cm 2).

7.8 Total Column CHOCHO

7.8.1 Operational Algorithm

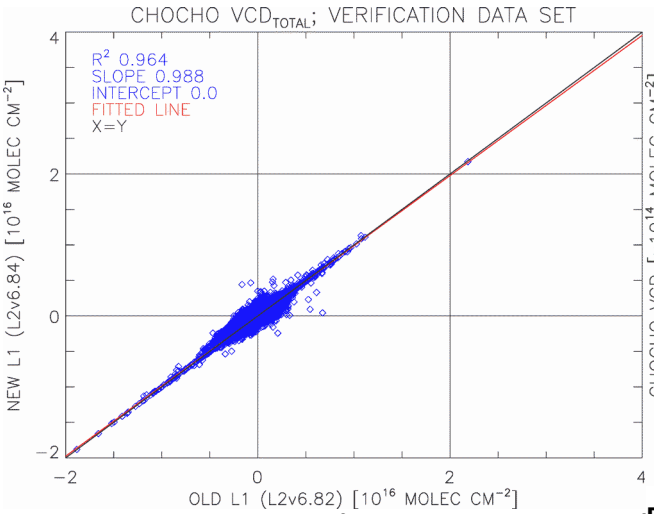

Figure 7.21: *Scatter plot for the total columns of CHOCHO*

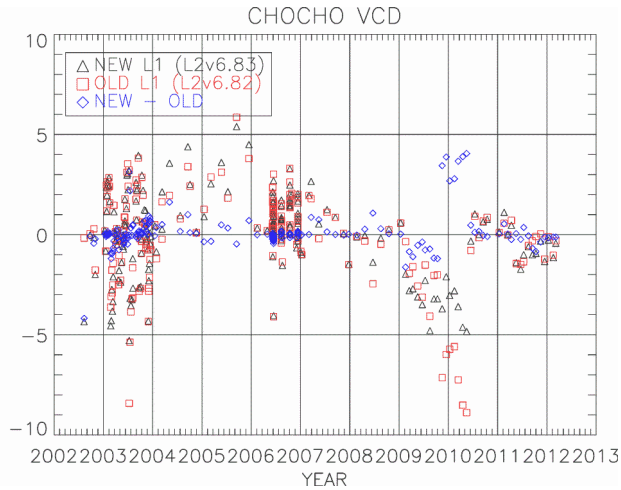

Figure 7.22: *Medians of CHOCHO total columns retrieved using L1v9 and L1v8 for each orbit as well as absolute differences between them as a function of time*

Glyoxal is one of the weakest absorbers among the SCIAMACHY products, which makes its retrieval a challenge. Furthermore it is retrieved from the Channel 3, where measurements were recorded with the shortest integration time. This leads to a large scatter in retrieved VCDs as seen in Figure 7.22. Nevertheless, the regression statistic is very good (Figure 7.21) and no temporal trend is introduced after the switch to the new L1.

8 Step 2 Verification AAIA/Clouds

8.1 AAIA

8.1.1 Operational Algorithm

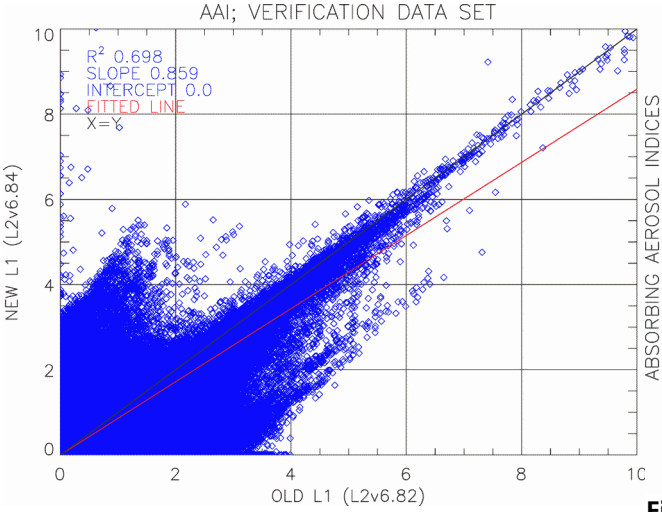

Figure 8.1: *Scatter plot for the absorbing aerosol index.*

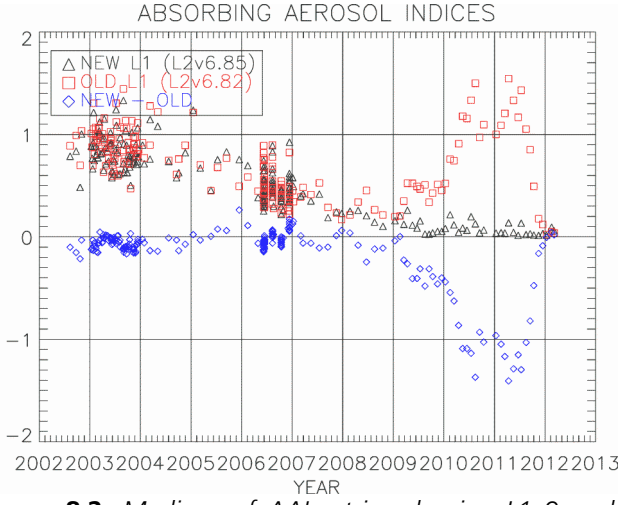

Figure 8.2: *Medians of AAI retrieved using L1v9 and L1v8 for each orbit as well as absolute differences between them as a function of time*

Starting from 2009 both versions goes apart: new L1 close to zero values, old L1 goes up, peaks in 2011 and then also close to zero. Both versions clearly do not behave as expected. The radiance in V.9 of the Level 1 product has changed significantlly. The large differences in shown in Figure 8.2 are mainly due the fact that the retrieval fails more often (or to be more precise: produce more negative residuals (at least in the verification data set) when Level 1 version 9 is used. If the retrieval fails, then in the old format the AAI was set to zero[2]. Looking at a scatter plot of the orbit median of the residuals calculated by the algorithm that are used to determine the AAI, we see that in cases where the residuals are positive, both versions agree reasonably well (see Figure 8.3).

2 In the new netCDF format the AAI is set to a fill value in this case

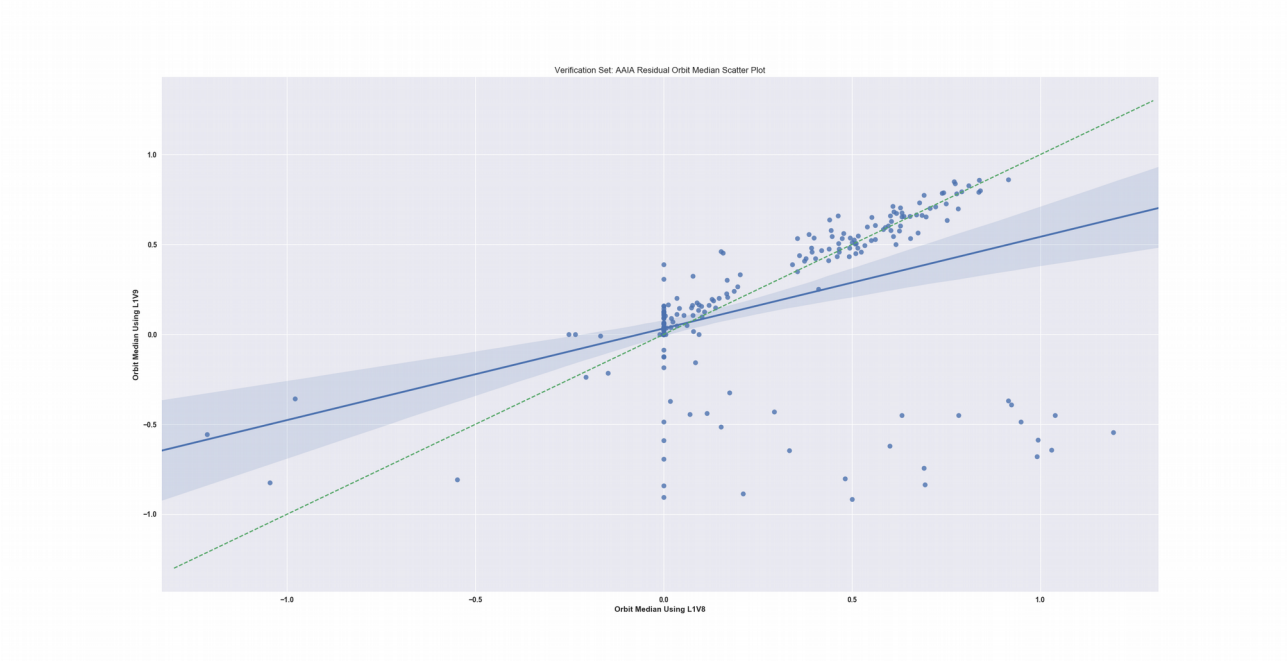

Figure 8.3: *Scatter plot of the orbit median residuals retrieved by the AAI algorithm when using Level 1 V9 (y-axis) and V8 (x-axis). The solid line shows the linear regression, the dotted line the one-to-one line. If one disregards negative residuals, V9 performs similar to V8.*

8.2 Cloud Fraction

8.2.1 Operational Algorithm

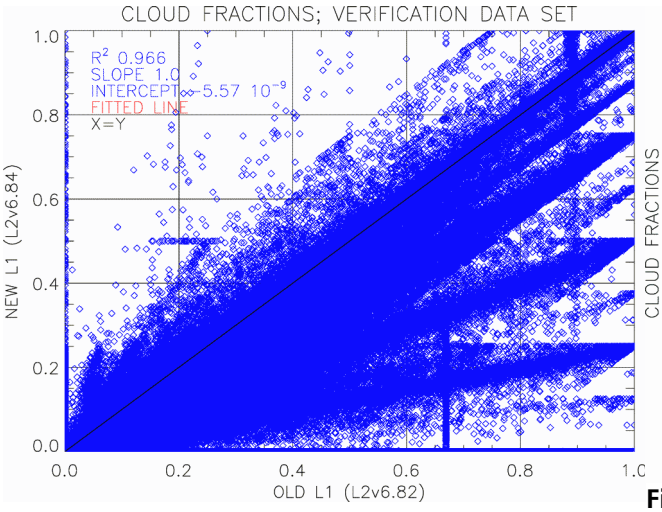

Figure 8.4: *Scatter plot for the cloud fractions*

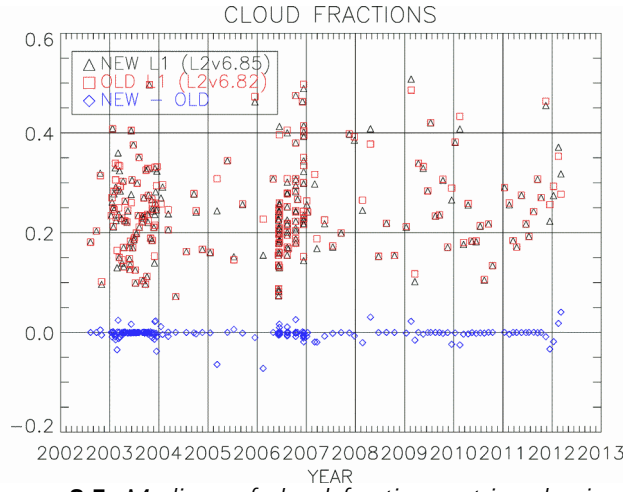

Figure 8.5: *Medians of cloud fractions retrieved using L1v9 and L1v8 for each orbit as well as absolute differences between them as a function of time*

In Figure 8.4 the scatter plot for cloud fractions is shown. Points laying outside X=Y-line (shown in black) corresponds to CFs in high latitudes, where for snow/ice covered surfaces higher CFs had been retrieved with the old L1 as an input. The new Level 1 data have more accurate PMD values which are

used by the algorithm. Therefore especially in the polar regions the separation of ice from clouds is improved. This leads to larger difference between the fractions retrieved using Level 1 V8 and Level 1 V9 data. Despite looking noisy in the figure such points represent only very limited fraction of the verification data set. That is why the regression statistic calculated for cloud fractions is still very good: R_2 = 0.966, slope = 1.0 and intercept very close to zero.

No time trend is observed for cloud fractions (Figure 8.5).

8.3 Cloud Top Height

8.3.1 Operational Algorithm

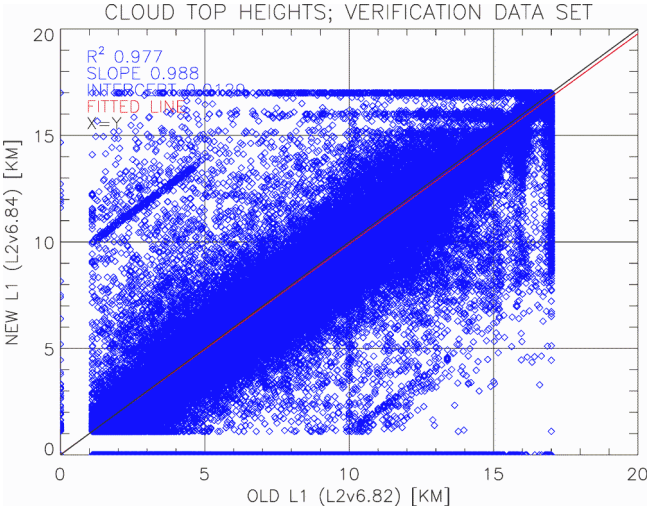

Figure 8.6: *Scatter plot for the cloud top heights.*

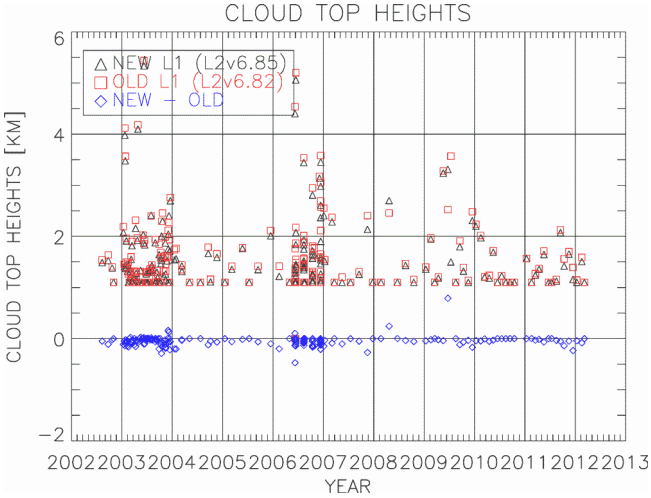

Figure 8.7: *Medians of cloud top heights retrieved using L1v9 and L1v8 for each orbit as well as absolute differences between them as a function of time*

The Pearson coefficient for both cloud top heights data set is 0.977, the slope is 0.988 and the intercept 12.9 meters. Considering that also no time trend is observed, the Step 2 verification for CTHs is successful.

9 Step 2 Verification SWIR Trace Gases

9.1 Total Column CH_4

9.1.1 Operational Algorithm

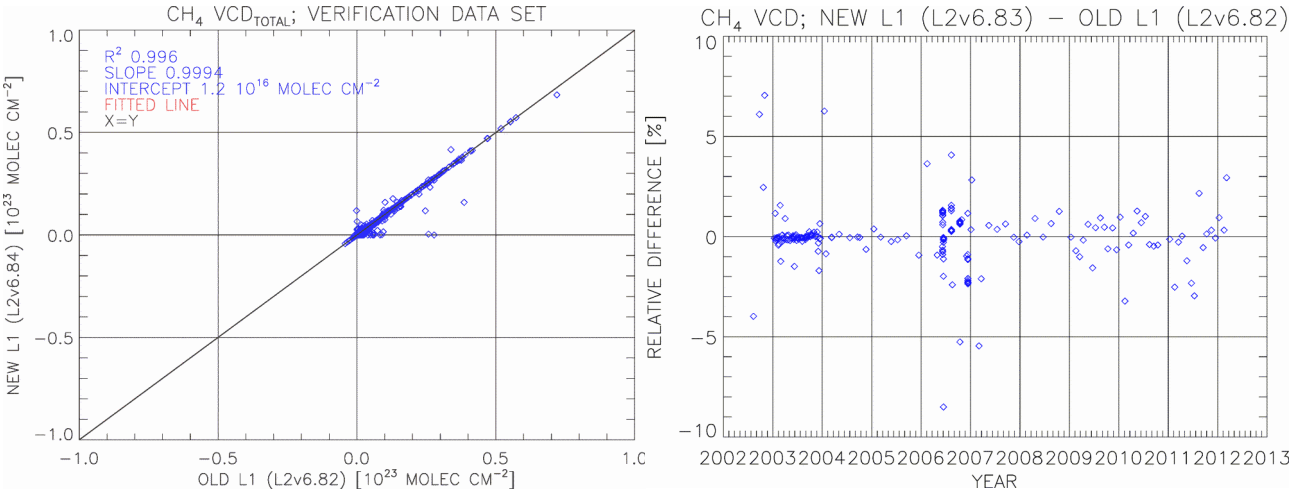

Figure 9.1: *Scatter plot and relative difference for V8 and V9 Level 1 input*

Taking into account all difficulties related to the methane retrieval (e.g. detector degradation in channel 6+ and very low SNR), there is an excellent agreement between both methane data sets.

9.2 Total Column CO

9.2.1 Operational Algorithm

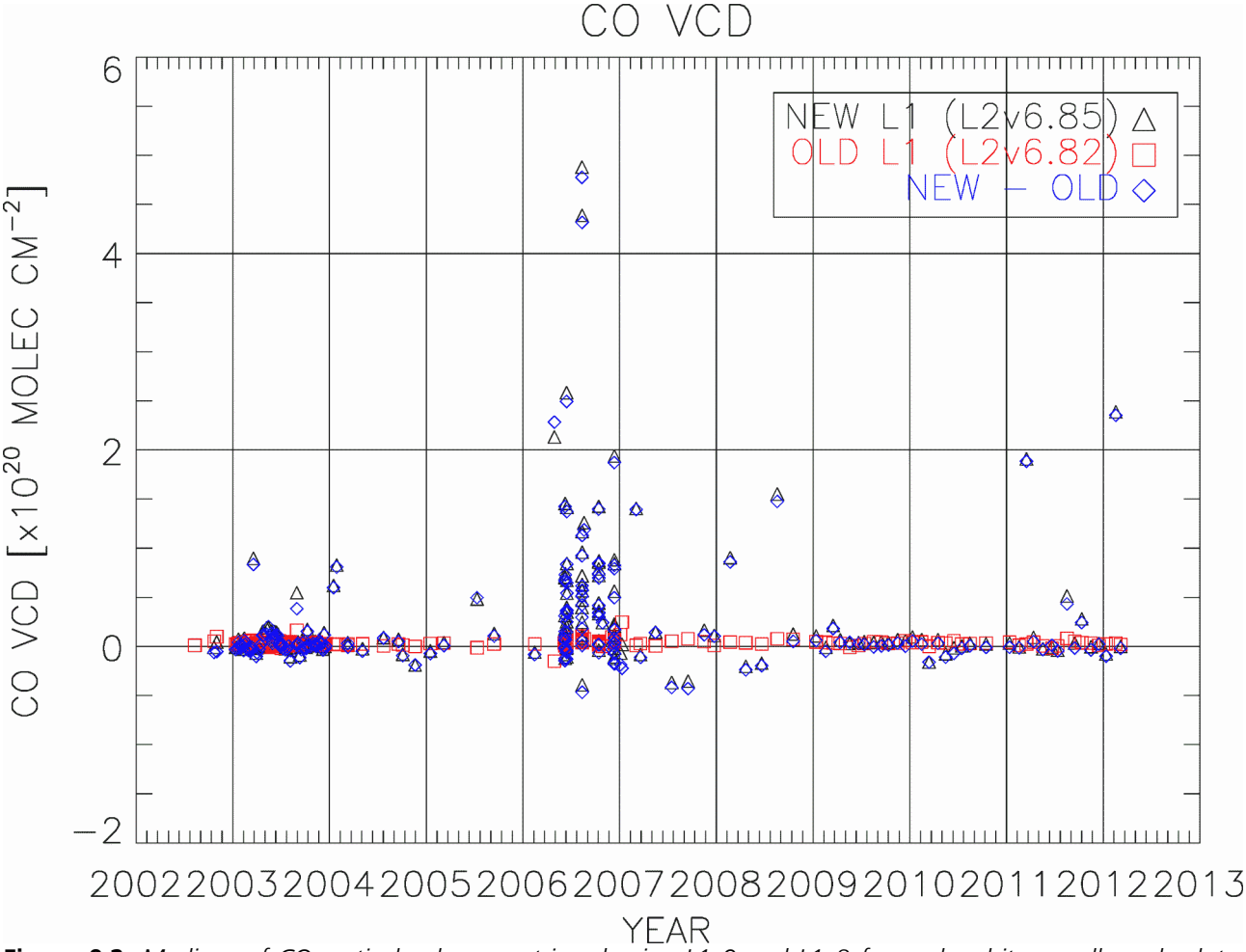

Figure 9.2: *Medians of CO vertical columns retrieved using L1v9 and L1v8 for each orbit as well as absolute differences between them as a function of time*

There is a clear issue with the L2 V7 data processed using the latest L1: contrary to the previous L2 v6.82 version (old L1) new results are 1-2 orders of magnitude higher than common physical CO values. This is not unexpected: The retrieval of CO in channel 8 is very difficult because of the weak CO signature, bad pixels and high background. The Level 2 algorithm was not changed, but the Level 1 processing in channel 8 was changed:

1. A new bad pixel mask was introduced for channel 8
2. A new spectral base axis was introduced for channel 8
3. A new dark calculation was introduced for channel 8
4. The radiometric calibration was updated for all channels

The histogram of filtered data for the whole verification set (Figure 9.3) shows that the V9 Level 1 product leads too much lower convergence and a CO value that is too high. Figure 9.5 shows the

orbit median for VCD1 (xCO, i.e. CO ratioed with CH_4) with nominal settings for version 8 Level 1 and version 9 Level 1 as input. Using the new mask for the operational retrieval leads to many more outliers and general worse convergence.

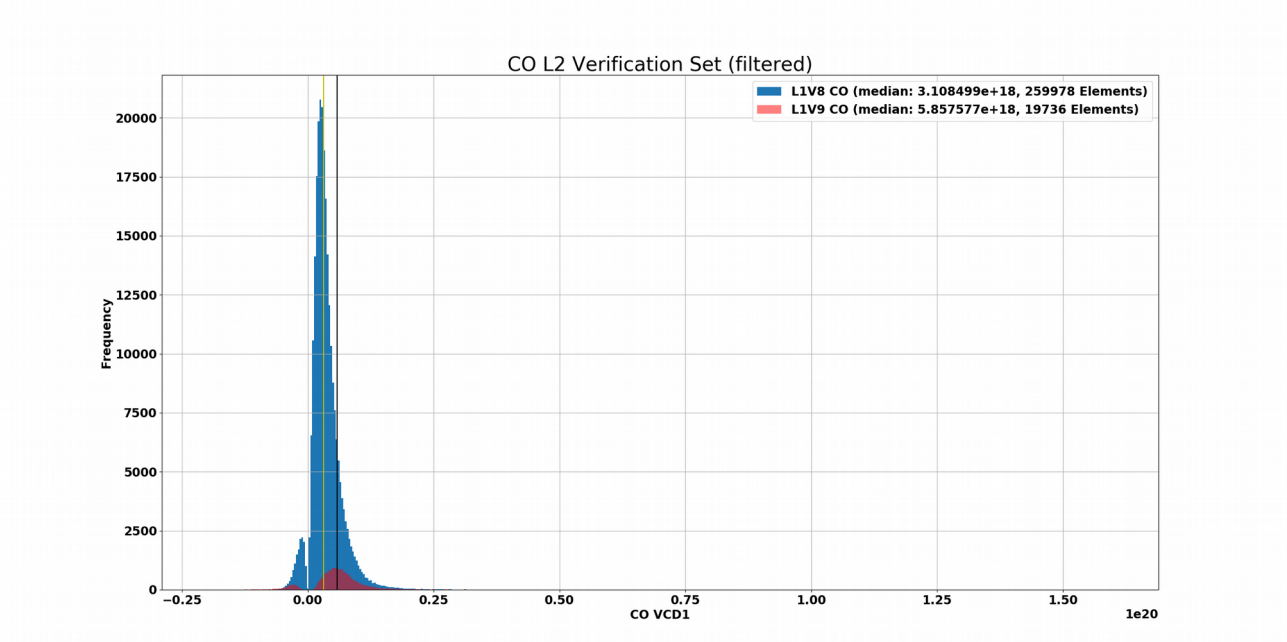

Figure 9.3: *Histogram of all CO values retrieved in the verification data set with V8 (blue) and V9 (red, transparent) Level 1 as input. The convergence rate with the new Level 1 is much lower.*

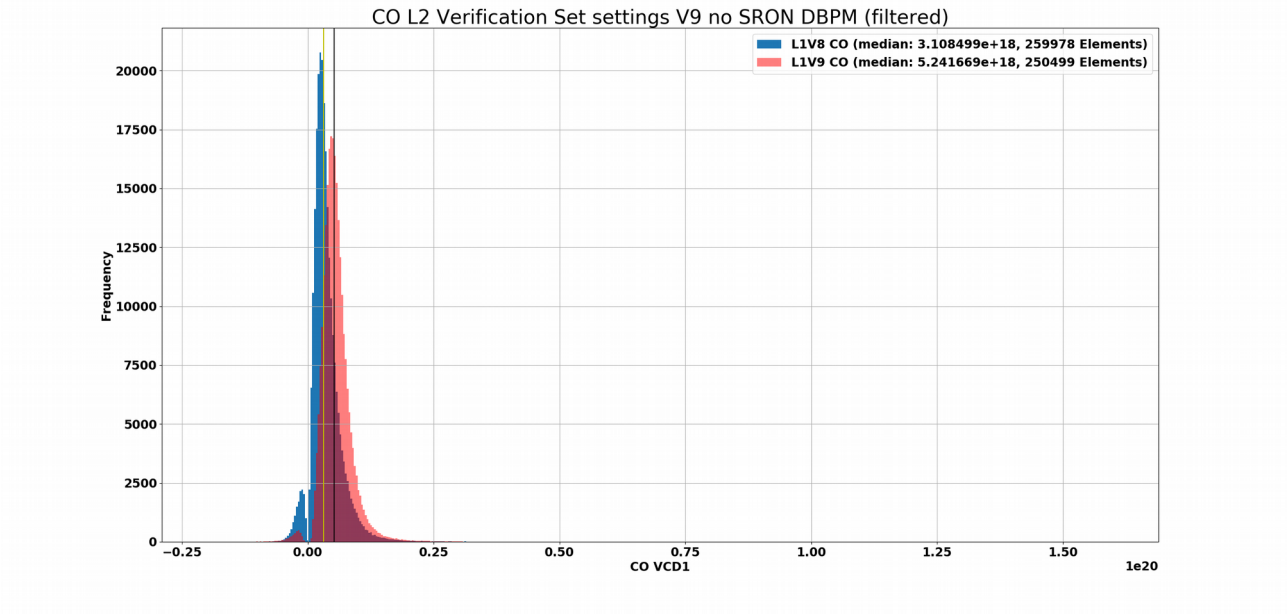

Figure 9.4: *Histogram of CO values from the verificaction set, but now using the original V8 bad and dead pixel mask (colors as in previous figure).*

Switching off the new mask in the retrieval and using the same mask as for the Level 1 V8 processor shows better convergence values (see Figure 9.4). However, the median values of the VCDs are higher than in the previous processing

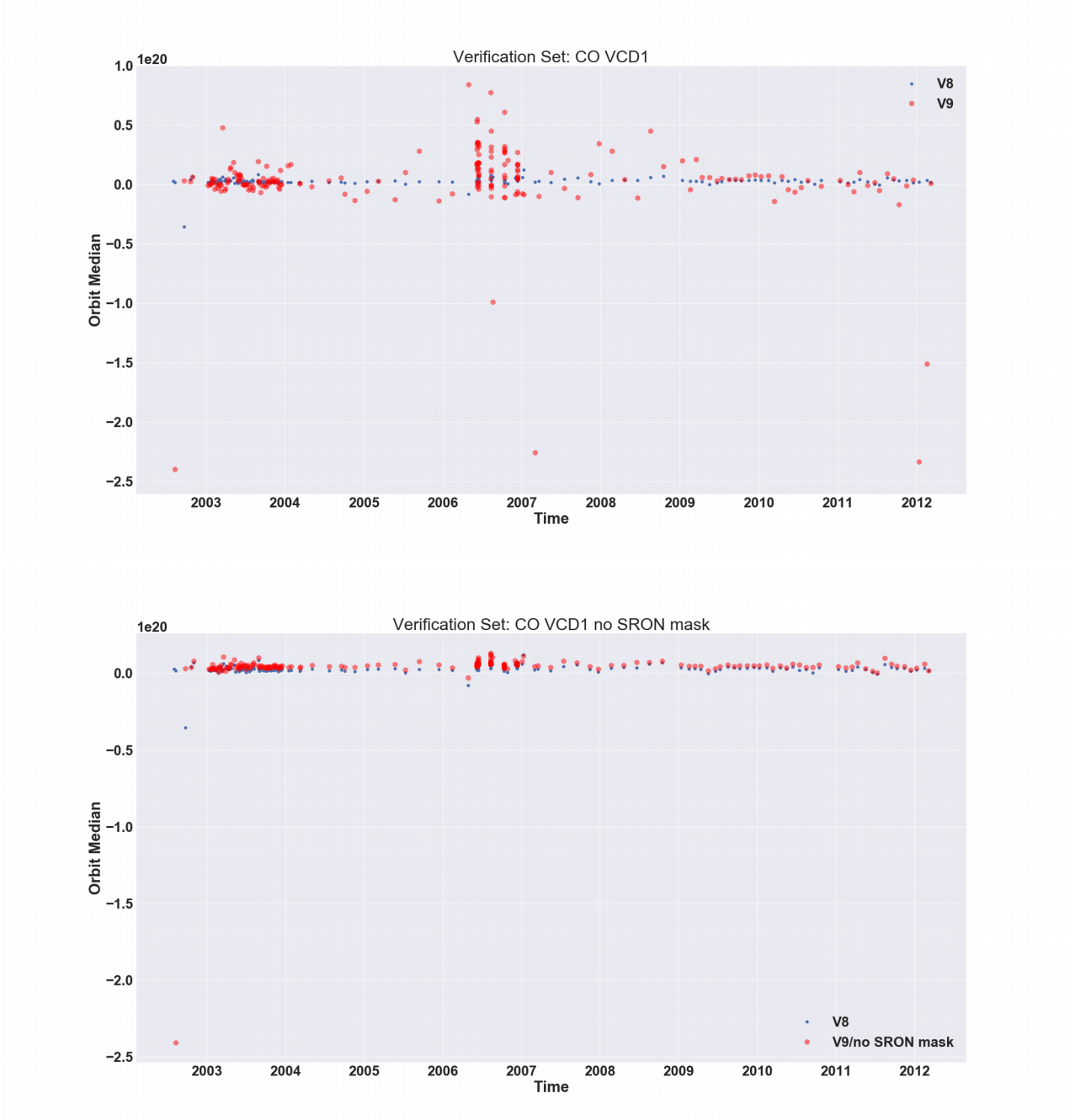

Figure 9.5: *Orbit medians of VCD1 using Level 1 V8 (blue) and V9 (red). Top nominal settings, bottom nominal settings without the new mask. The y-scale of the figures are similar with the right being slightly zoomed in.*

The results triggered a more thorough investigation. Different configurations for the generation of Level 1 and Level 2 and their combinations were tested w.r.t their impact on CO:

Level 1 Settings	Level 2 Settings
Standard (new mask used, new spectral calibration used)	Standard (as in V. 6.01)
No new Mask: as standard without new mask	As in V5.02 (previous L2 version)
No new mask, no new spectral calibration	Similar to prototype (which uses an evolved algorithm compared to the currently operationally implemented one).

The best two combinations were

1. *L1 No new mask and no new spectral calibration, L2 Standard:* This combination reproduced for the verification set the results of the currently operational retrieval (see Figure 9.6).
2. *L1 No new mask, L2 settings as in Version 5.02 of the L2 processor:* This combination produced higher CO values. Previous investigations with the prototype gave hints that higher CO values might be more realistic.

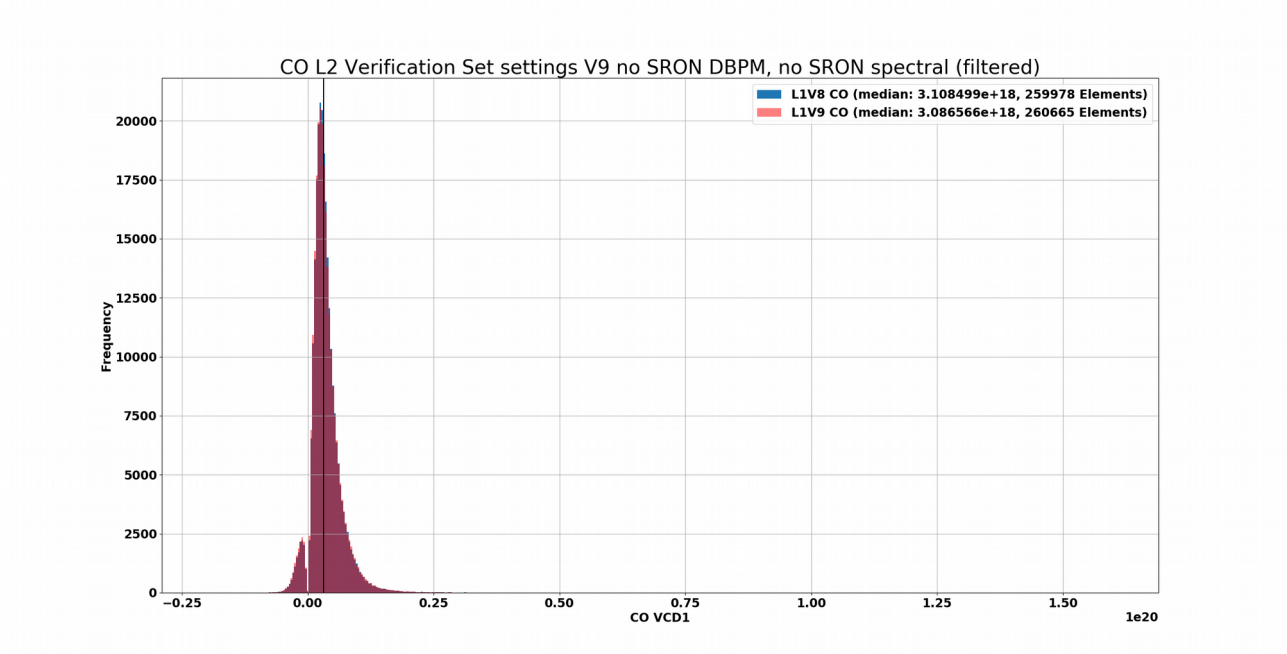

Figure 9.6: *Histogram for the case of not using the new bad pixel mask and also not using the new spectral calibration in channel 8. This reproduces the previous CO retrieval result for the verification set.*

In order to decide between these two options we processed 2 months of 2004 and compared the results with ground stations in Toronto and Bremen. The stations were selected because of the relative homogeneous terrain in the surrounding areas.

The comparison shows that option 1 (no new mask and no new spectral calibration) matches the data of these 2 stations better than the other option. In order to come to not delay the re-processing further we used the already available Level 1 V8/Level 2 V6.01 to represent option 1. This is justified because option 1 with Level 1 V9/Level 2 V7 reproduces the results of L1V8/L2V6.01, see Figure 9.6 in distribution and – except a very small delta – in value. The difference in option 1 and option 2 is in any case much larger than the small difference in using V9/V7 or V8/V6. Thus the method is adequate for this comparison.

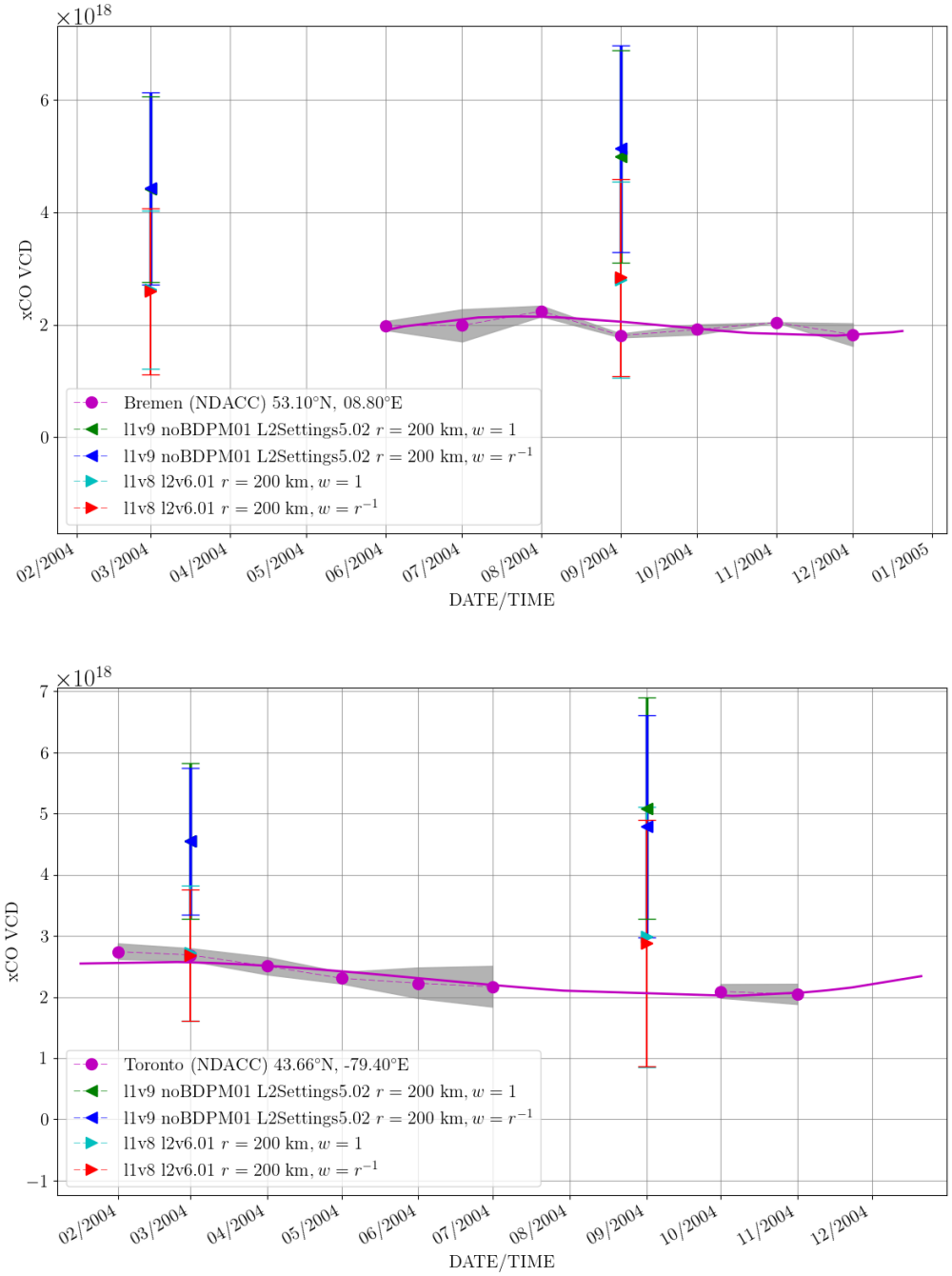

Figure 9.7: Comparison of monthly mean of two NDACC stations Bremen (top) and Toronto (bottom) and the two processing options: L1V8 results (option 1) red/cyan, Option 2: blue/green. W = r^{-1}, (1) weighting of results with (without) distance.

In view of these results and the fact that CO is the only operational product in channel 8, *it was decided to go back to the old bad pixel mask and use the previous spectral calibration in the Level 1 processing.* The new Level 1 product is still an improvement over V8, since the dark correction and the radiometric calibration were updated. Only a validation based on a large data set will show the quality

of CO and the effect of the new Level 1. However, this is out of scope for the verification.

10 Step 2 Verification Tropospheric Gases

10.1 Tropospheric NO_2

10.1.1 Operational Algorithm

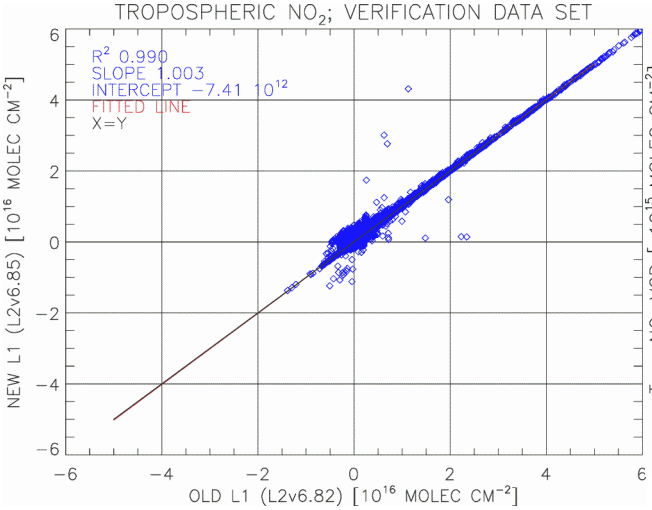

Figure 10.1: *Scatter plot for the tropospheric NO2.*

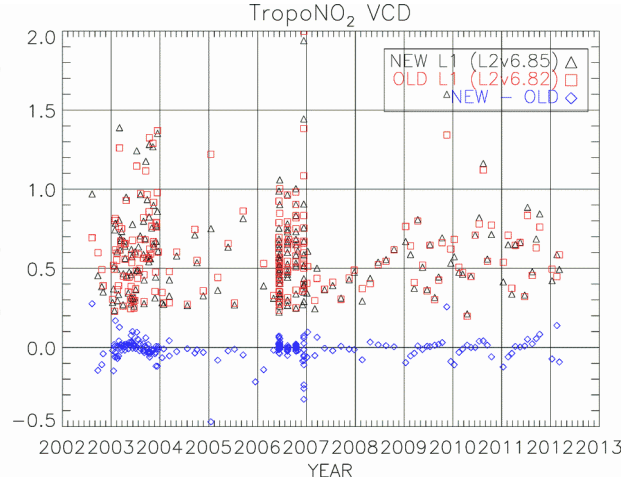

Figure 10.2: *Medians of tropospheric NO2 columns retrieved using L1v9 and L1v8 for each orbit as well as absolute differences between them as a function of time.*

The impact of the new L1 on the tropospheric NO_2 product has been checked as well. The product remains to be of high quality.

10.2 Tropospheric BrO

10.2.1 Operational Algorithm

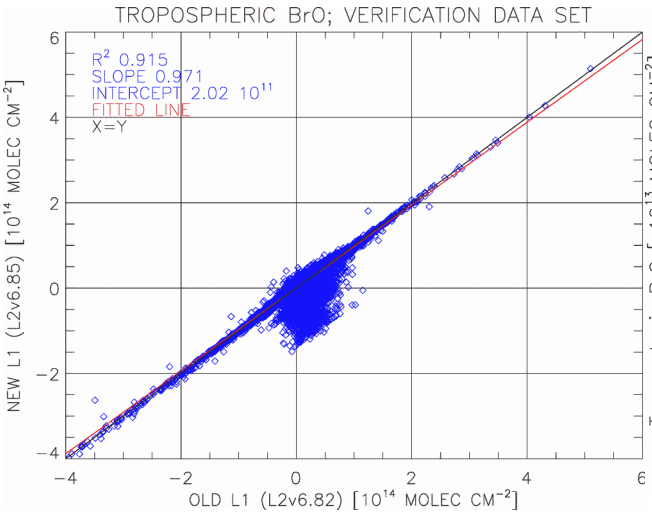

Figure 10.3: *Scatter plot for the tropospheric BrO.*

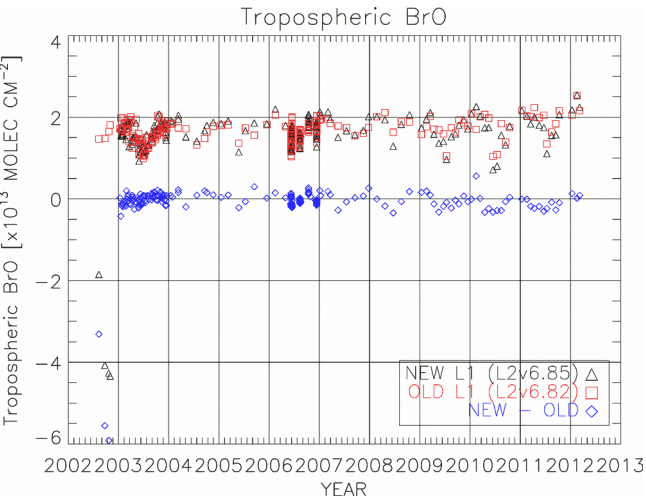

Figure 10.4: *Medians of tropospheric BrO columns retrieved using L1v9 and L1v8 for each orbit as well as absolute differences between them as a function of time.*

Since the tropospheric BrO product is very closely related to the total BrO columns, the orbits from Year 2002 are also affected in the very same way as the total BrO. This is the only shortcoming found after the switch to the new L1.

11 Step2 Verification Limb Trace Gases

11.1 O_3 Profiles

11.1.1 Operational Algorithm

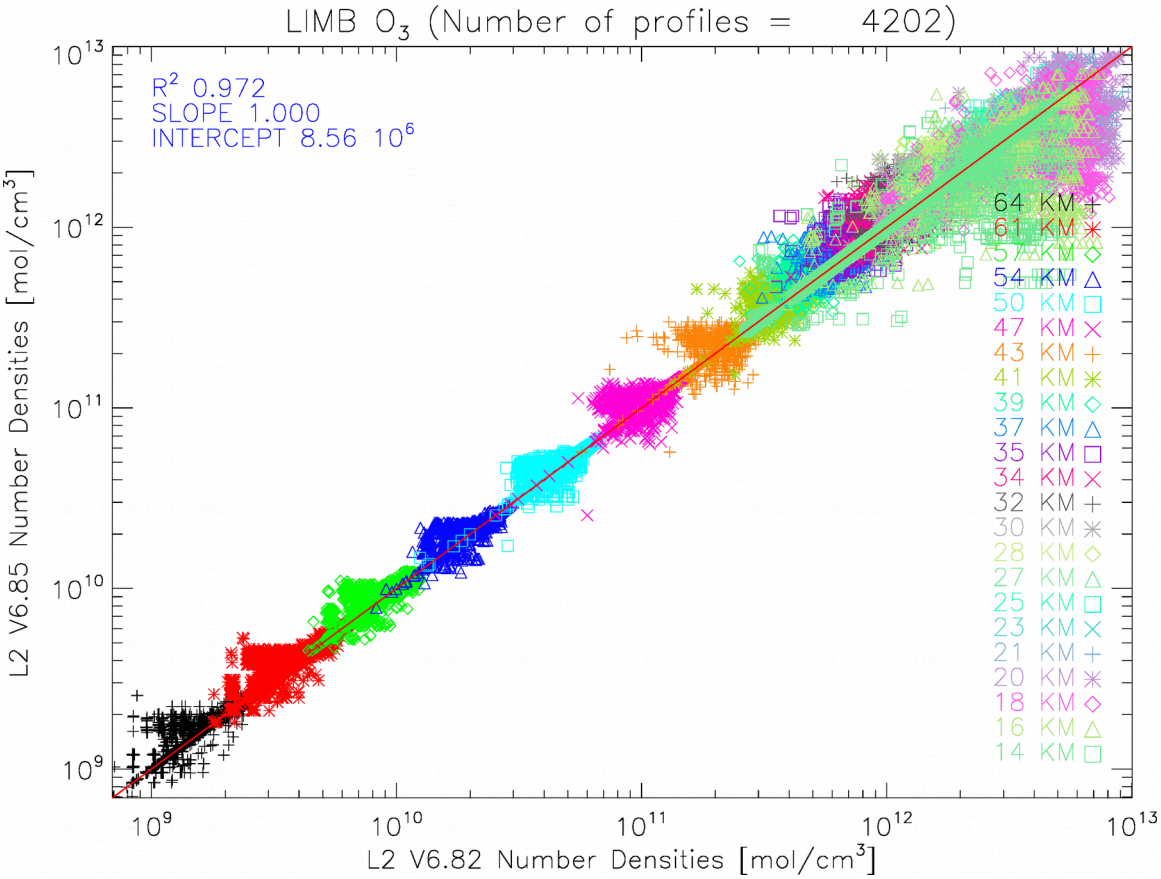

Figure 11.1: *Scatter plot for O3 profiles retrieved using L1v8 (x-axis) and L1v9 (y-axis)*

The scatter plot for ozone profiles retrieved from the L1v8 and L1v9 is shown in Figure 11.1. Different altitudes are colour coded. The difference between the two data sets is very small.

11.2 NO_2 Profiles

11.2.1 Operational Algorithm

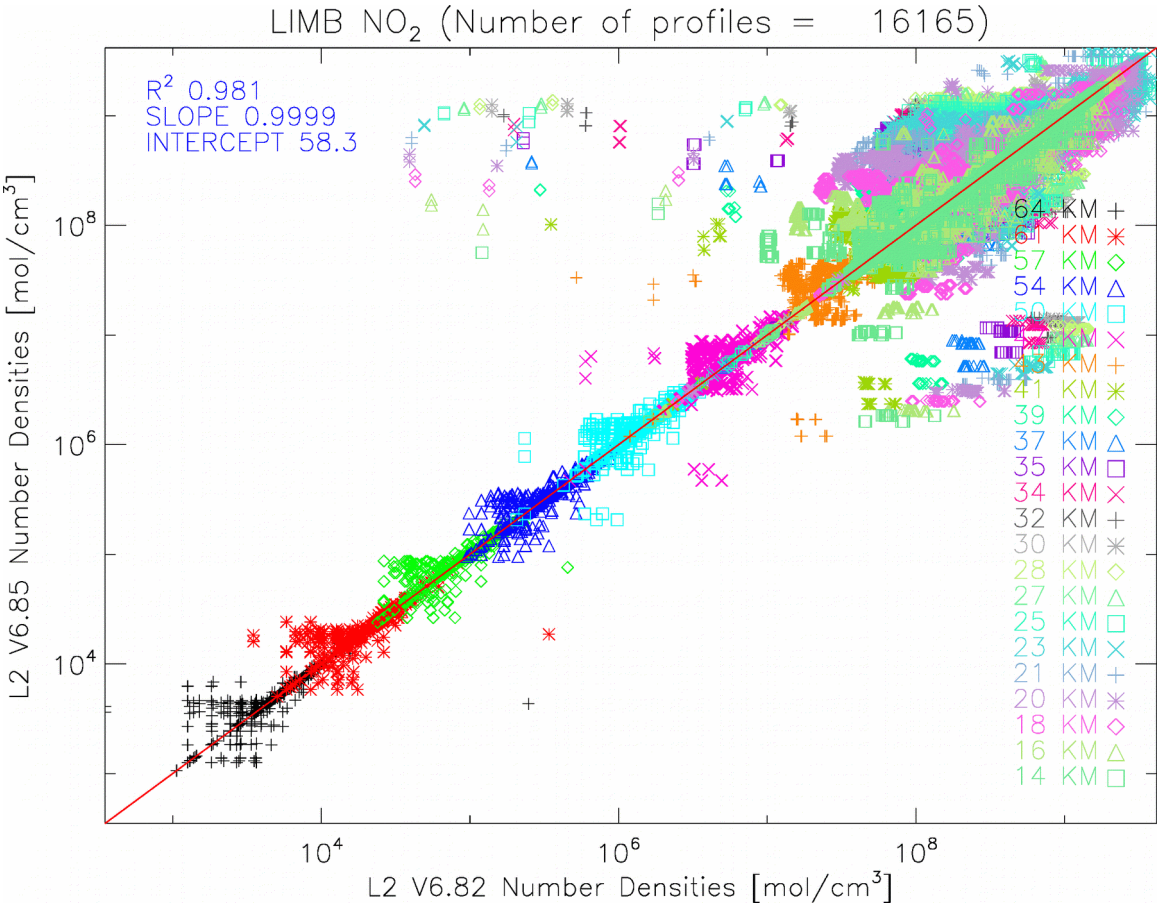

Figure 11.2: *Scatter plot for NO2 profiles retrieved using L1v8 and L1v9*

The scatter plot for NO2 profiles retrieved from both versions of the L1 files is shown in Figure 11.2. The agreement is very good.

11.3 BrO Profiles

11.3.1 Operational Algorithm

Figure 11.3 shows a scatter plot for BrO profiles retrieved from the L1v8 and L1v9. The correlation coefficient is very high (0.96). Also it is important that no bias is to be seen. The BrO retrieval is

generally very sensitive to any change, because of lower signal-to-noise ratio than for the other two limb products and considering that the observed agreement is excellent.

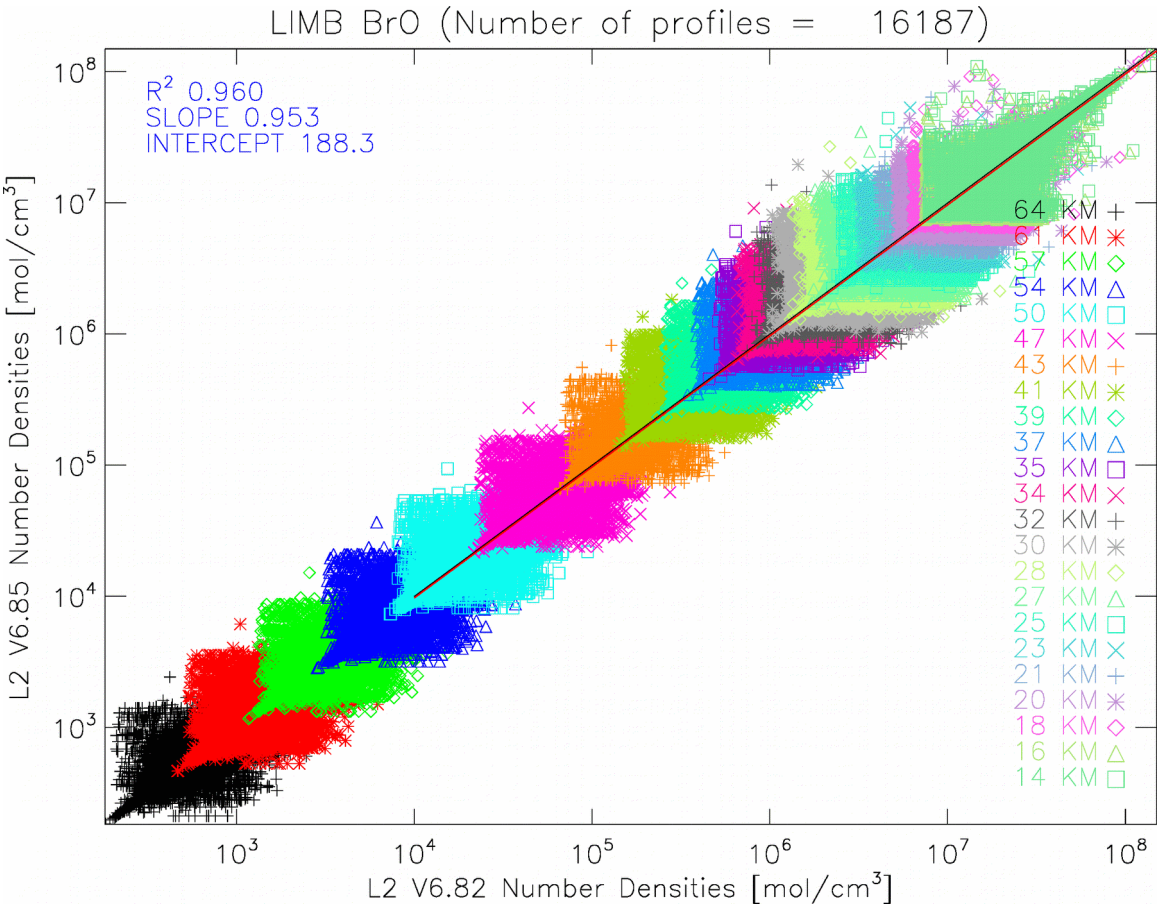

Figure 11.3: Scatter plot for BrO profiles retrieved using L1v8 and L1v9

11.4 Tangent Height Dependencies

In Figures 11.4, 11.5 and 11.6 one can see that the correlation, at different heights, between the two Level 2 profiles of O3, NO2, and BrO respectively is higher than 0.7 in O3 and BrO cases and higher than ~0.8 in NO2. There is an obvious correlation between the number densities obtained from Lv8 and L1v9 at all heights. Nevertheless the interpretation of the corresponding coefficient behaviour as a function of the height is not yet obvious.

On the other hand, the slope coefficients are equal to ~1 most of the time. It shows that the number densities increase simultaneously independently of the height in the atmosphere. BrO case is somewhat different, the coefficient is mainly < 1, possibly due to the large errors from the retrieval.

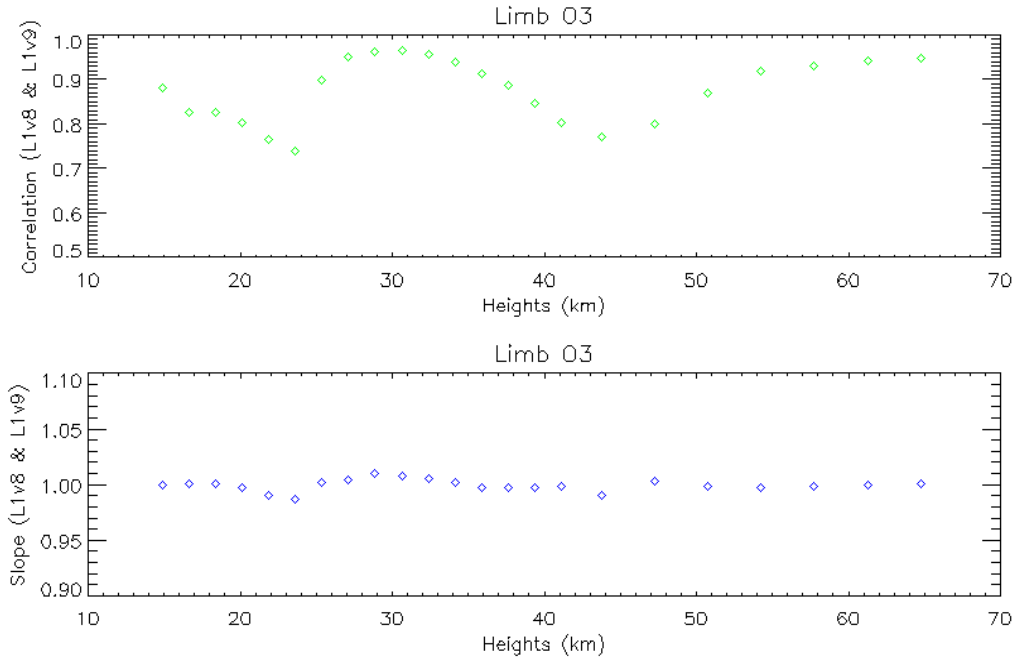

Figure 11.4: *Correlation (top) of limb Level 2 O3 number densities between the ones obtained from L1v8 and from L1v9 as a function of height. The bottom plot is the slope coefficient of the densities, when plotted against each other, as a function of height.*

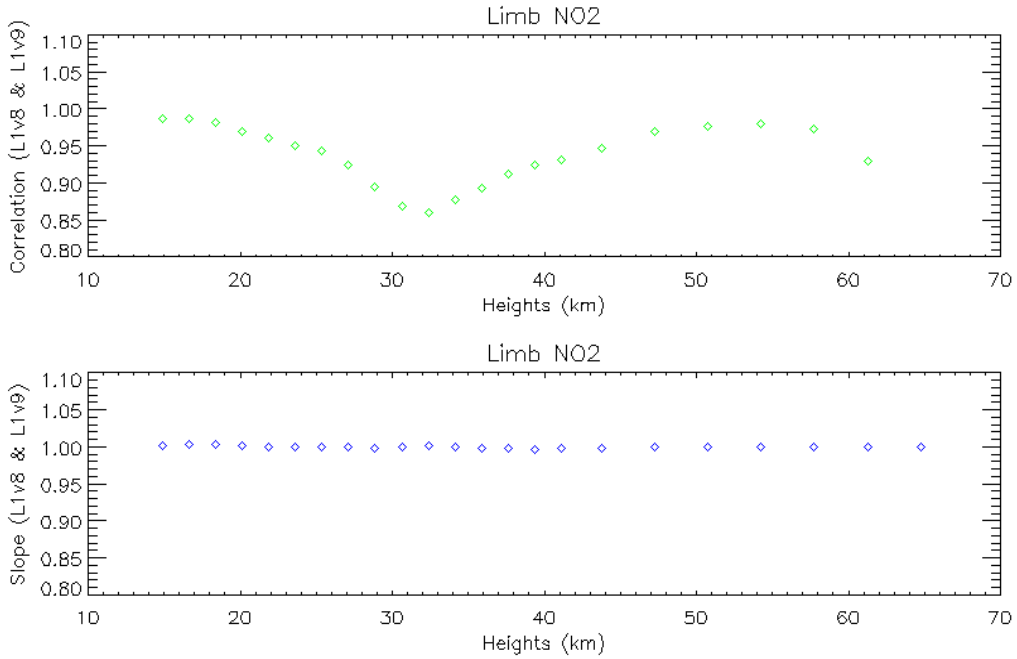

Figure 11.5: *Similar to Figure 11.4 but for NO2 gas.*

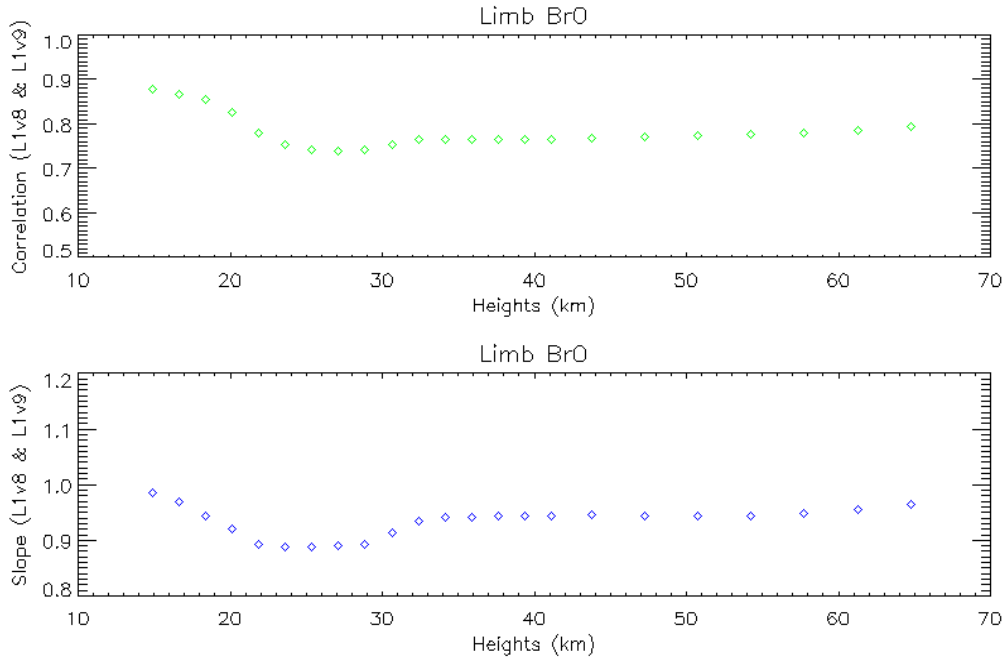

Figure 11.6: *Similar to Figure 11.4 but for BrO gas*

There is clearly a consistency between the two retrieved level 2 densities. Deviations are however expected due to the new updated spectra in Level 1. Nevertheless, the observed variations as a function of heights may need further investigation.

11.5 Cloud Products:

The following parameters from the Limb Clouds MDS were compared:

- Cloud flags (water, ice clouds, polar stratospheric clouds (PSCs), and noctilucent clouds (NLCs));
- Maximum values of colour index ratios (CIRs) for water and ice clouds, as well as PSCs;
- Heights of maximum values of CIRs for all four type of clouds.

The total number of obtained and analysed limb profiles is 19,731.

11.5.1 Operational

The cross tables 11.1 to 11.4 deliver a detailed picture for limb clouds flags. For each combination of cloud flag values the number and percentage of total records with that combination is given. The blue grey shades cells show the number where the results from L1b V8 and L1b V9 generated L2 products agree. For a few records differences in cloud flags were found:

- water clouds: 124 records (0.6%);
- ice clouds: 214 records (1.08%);

- PSCs: 10 records (0.05%);
- NLCs: 22 records (0.11%).

	v9			
v8	**0**	**1**	**2**	**3**
0	1,391(7%)	27(0.14%)	1	4
1	13(0.1%)	11,773(60%)	49(0.25%)	2
2	1	17(0.1%)	4,273(22%)	1
3	7	1	1	178(0.9%)

Table 11.1: Flags for water clouds retrieved from L1v8 and L1v9.

0 - no clouds
1 - partially cloudy
2 - fully cloudy
3 - bad data or cloud top height too high

	v9		
v8	**0**	**1**	**2**
0	5,817(29.5%)	140 (0.7%)	2
1	64(0.3 %)	13,633(69.1%)	4
2	3	1	67(0.3%)

Table 11.2: Flags for ice clouds retrieved from L1v8 and L1v9.

0 - Water cloud
1 - ice cloud
2 - bad data (MAXHEIGHT_ICL is greater than the warning tangent height)

	v9	
v8	**0**	**1**
0	19,349(98.1%)	8
1	2	372(1.9%)

Table 11.3: Flags for PSCs retrieved from L1v8 and L1v9.

0 - no PSC
1 - PSC

	v9			
v8	**0**	**1**	**2**	**3**
0	17,611 (89.3%)	1	4	1
1	8	280(1.4%)	1	1
2	1	1	418(2.1%)	1

3	1	1	1	1,410(7.1%)

Table 11.4: Flags for NLCs retrieved from L1v8 and L1v9.

0 - no NLC
1 - NLC criterion 1 fulfilled (radiance increase with height)
2 - NLC criterion 2 fulfilled (radiance ratios above threshold)
3 - both NLC criteria fulfilled

Figures 11.7 and 11.8 (below) show the scatter plots of the CIRs for water clouds and PSCs' respectively. There is a very good agreement between the two versions from L1v8 and L1v9. This is tested with the correlation that is higher than 0.99 as well as the fitted linear function where the slope is higher than 0.98.

Figure 11.9 shows the CIRs for ice clouds. There is a clear disagreement between the two Level 2 datasets, as also seen in the low correlation value of ~0.16. After investigating this particular disagreement, it turned out that it stared to occur around fall 2009. In fact, until September 2009 there is a very good agreement as seen in figure 11.10 with a correlation of ~0.98. Beyond that date the divergence increases and gets worse over time as shown in figures 11.11 and 11.12 with a correlation dropping from ~0.74 to ~0.47. The peculiarity occurs or begins at about the same time where the AAI shows its peculiar values.

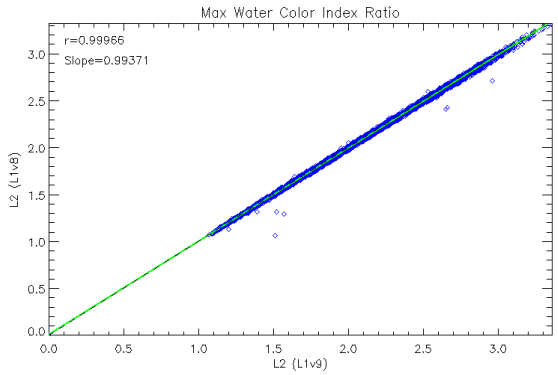

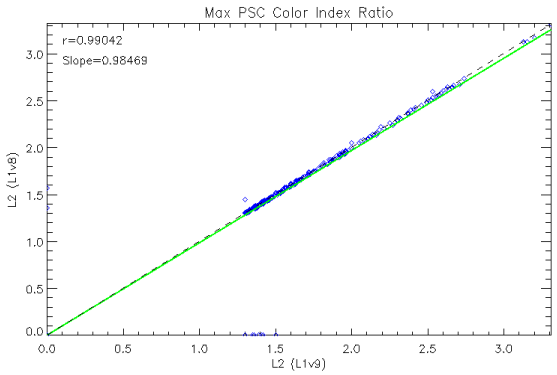

Figure 11.7: Scatter plot for water clouds maximum CIRs

Figure 11.8: Scatter plot for PSCs' maximum CIRs

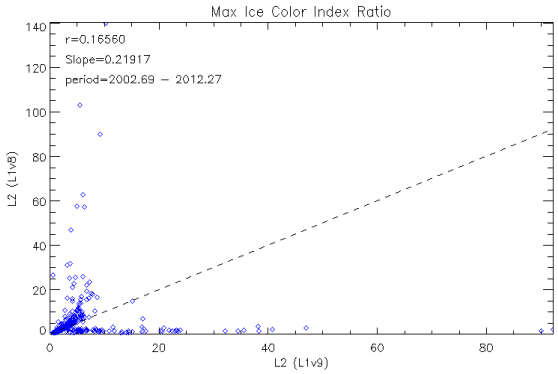

Figure 11.9: Scatter plot for ice clouds maximum CIRs (over the entire lifetime of the mission)

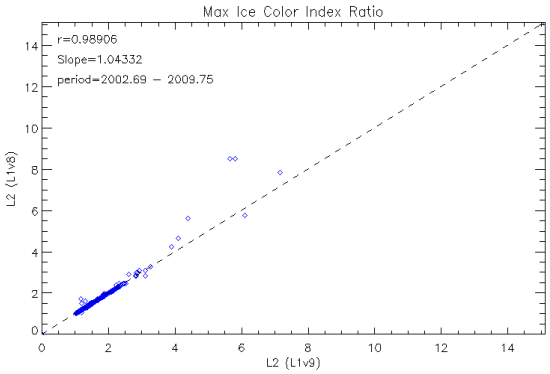

Figure 11.10: Similar to Figure 11.9 but here it covers the mission until September 2009.

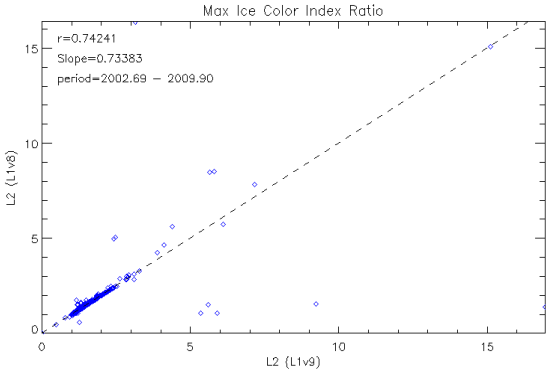

Figure 11.11: Similar to Figure 11.9 but here it covers the mission until November 2009.

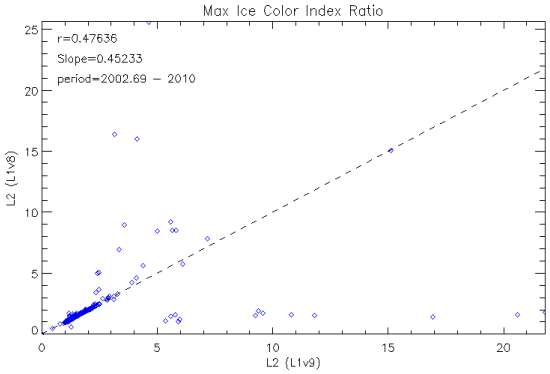

Figure 11.12: Similar to Figure 11.9 but here it covers the mission until 2010

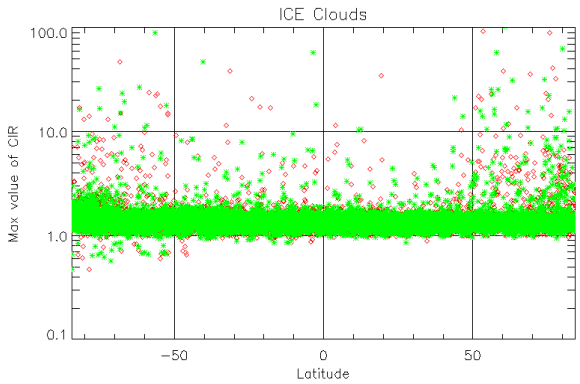

Figure 11.13: Ice Clouds CIRs between L2 retrieved from L1v9 (red) and L1v8 (green) as a function of latitude.

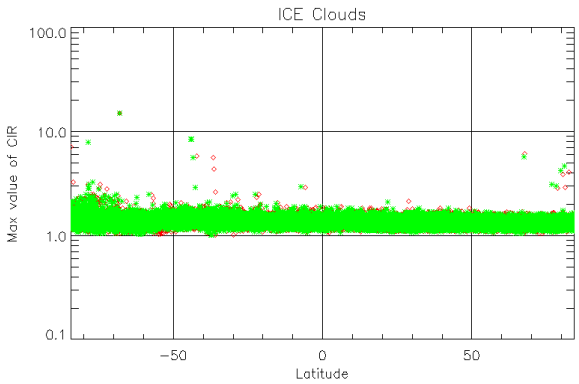

*Figure 11.14: Similar to figure 11.13 but here the data cover the mission time frame until **September 2009**.*

Figures 11.13 and 11.14 show the Ice clouds' CIR comparison of both datasets as a function of latitude. Figure 11.14 however covers the mission time frame until September 2009. In the later one, the figure shows less mismatches between the values compared to 11.13's. This is consistent with the agreement seen between the two datasets in 11.10 that also ends in September 2009. Still the altitude for the maximum CIR agrees in most cases betweeen the 2 versions.

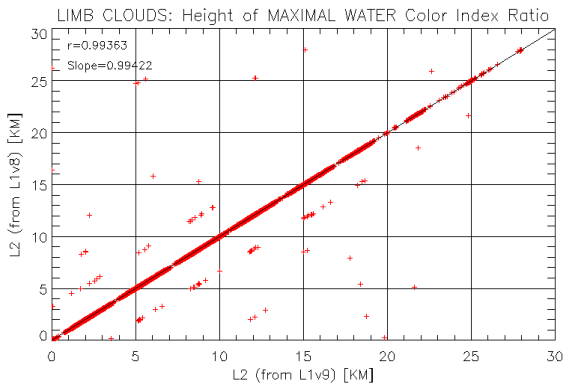

Figure 11.15: Scatter plot for heights of maximum CIRs for water clouds.

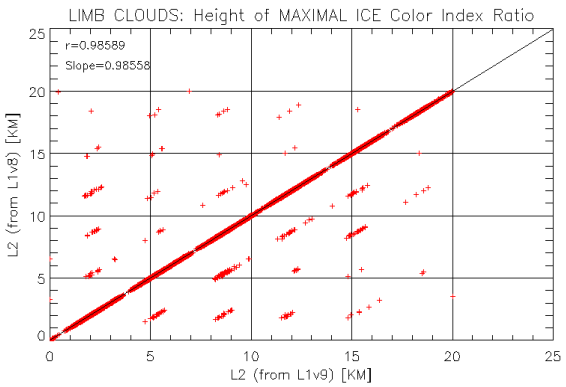

Figure 11.16: Scatter plot for heights of maximum CIRs for ice clouds.

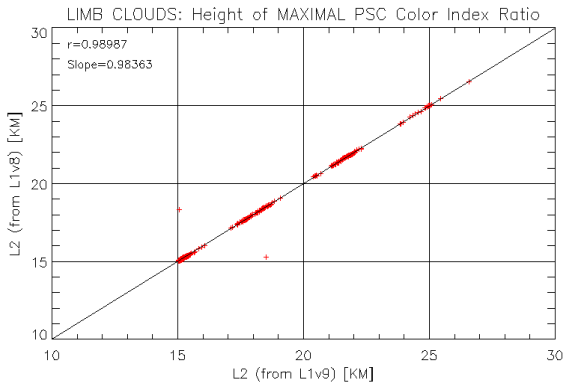

Figure 11.17: Scatter plot for heights of maximum CIRs for PSCs.

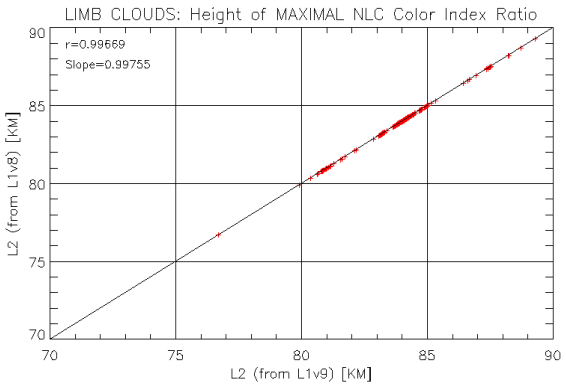

Figure 11.18: Scatter plot for heights of maximum CIRs for NLCs.

Figures 11.15 to 11.18 show an overall consistency of the height of the maximal CIR over different areas between both datasets obtained from L1v9 and L1v8. This is quantified with the very good correlation value > 0.98. The case of water and the ice in particular show several outliers and data points that leave the linear curve of the datasets' heights. .
A first look at the data as a function of time did not show specific time frames or orbits where such discrepancies suddenly or fully happen, but the amount of these mismatches increases over time.

12 Summary & Conclusions

The verification was successful. However, sue to the large changes to Level 1 data, some changes between the Level 2 products generated using Level 1 V8 and Level V9 could be observed (note that the changes stem solely from the different Level 1 radiances, the Level 2 algorithms were not changed in these cases). It is not possible to judge the truth of the changes based on the limited verifcation data set, because for the analysis a the whole missiondata set or independent validation measurements are needed. Therefore the following points should be investigated once the whole data set (or a sufficient sub-set) is available:

1. **Trend in Nadir O3 data:** While there is no trend visible in the individual O3 total columns from Level 1 V8 and Level 1 V9, the difference shows at least 3 different "plateaus" over time. However, the verification data are not dense enough and the distribution over time is not good enough to judge if there is a real trend.
2. **Total BrO:** The reason for the disagreement between Level 1 V8 and Level 1 V9 generated data was a calibration data base that still contained erroneous ASM diffuser measurements. The comaprison after 2002 shows a good agreement.
3. **AAI:** The AAI algorithm itself was not changed. However, since the Level 1 radiances were changed in V9, one can see a siginificant difference between the AAI values for this version and the previous version. In the verification data set, the retrieval seem to produce more often negative residuals. However, in cases were the retrieval is successful, both versions agree reasonably well. An investigation using the whole mission is recommended to assess tha quality of the AAI after the Level 1 change.
4. **Limb Clouds:** Overall good agreements between the two Level 1 versions. It seems that towards the end of 2009 the maximum ice CIR start to diverge from each other. However, the classification of the clouds agrees to a large degree in both data sets: In only 1.08% of the cases the classification was different. The altitude of the maximum CIR is also mostly the same. For the latter parameter, water clouds and ice clouds show some outliers. The reason for the difference could not be found with the limited data set available.